Somatic Mutations in Clonally Expanded T-lymphocytes in Patients with Chronic Graft-Versus-Host Disease

Giljun Park[1,2], Daehong Kim[1,2], Jani Huuhtanen[1,2], Sofie Lundgren[1,2], Rajiv K. Khajuria[1], Ana M. Hurtado[3], Cecilia Muñoz-Calleja[4], Laura Cardeñoso[5], Valle Gómez-García de Soria[6], Tzu Hua Chen-Liang[3], Samuli Eldfors[7], Pekka Ellonen[7], Sari Hannula[7], Oscar Bruck[1,2], Anna Kreutzman[1,2], Urpu Salmenniemi[8], Tapio Lönnberg[9], Andres Jerez[3], Maija Itälä-Remes[8], Mikko A. I. Keränen[1,2,10], and Satu Mustjoki, MD[1,2]

[1]*Hematology Research Unit Helsinki, Helsinki University Hospital Comprehensive Cancer Center, Helsinki, Finland*
[2]*Translational Immunology Research Program and Department of Clinical Chemistry and Hematology, University of Helsinki, Helsinki, Finland*
[3]*Hematology and Medical Oncology Department, Hospital Morales Meseguer. Centro Regional de Hemodonación. Universidad de Murcia. IMIB, MURCIA, Spain*
[4]*Department of Immunology, Hospital Universitario de La Princesa, Instituto de Investigación Sanitaria Princesa, Madrid, Spain*
[5]*Department of Microbiology, Hospital Universitario de La Princesa, Instituto de Investigación Sanitaria Princesa, Madrid, Spain*
[6]*Department of Hematology, Hospital Universitario de La Princesa, Instituto de Investigación Sanitaria Princesa, Madrid, Spain*
[7]*Institute of Molecular Medicine Finland (FIMM), University of Helsinki, Helsinki, Finland*
[8]*Turku University Hospital, Stem cell transplantation unit, Turku, Finland*
[9]*Turku Centre for Biotechnology, University of Turku and Åbo Akademi University, Turku, Finland*
[10]*Department of Hematology, Helsinki University Hospital Comprehensive Cancer Center, Helsinki, Finland*

Corresponding author:

Prof. Satu Mustjoki
Hematology research unit Helsinki,
University of Helsinki and
Helsinki University Hospital Comprehensive Cancer Center
P.O. Box 700, Haartmaninkatu 8
FIN-00029 Helsinki, Finland
e-mail: satu.mustjoki@helsinki.fi
Tel +358 9 471 71898, fax +358 9 471 71897

ABSTRACT

Graft-versus-host-disease (GvHD) is the main complication of allogeneic hematopoietic stem cell transplantation. GvHD patients have aberrant T cell expansions, which are thought to drive pathological immune activation. Here we report mechanistic insights that somatic mutations may account for persistent clonal T cell expansions in chronic GvHD (cGvHD). In an index patient suffering from cGVHD, we discovered persisting somatic *MTOR*, *NFKB2*, and *TLR2* mutations in an expanded CD4+ T clone. In the screening cohort (n=135), the *MTOR P2229R* kinase domain mutation was detected in two additional cGvHD patients, but not in controls. Functional analysis of the discovered *MTOR* mutation indicated a gain-of-function alteration in translational regulation yielding in up-regulation of phosphorylated S6K1, S6, and AKT. Paired single-cell RNA and T cell receptor alpha and beta sequencing strongly supported cytotoxicity and abnormal proliferation of the clonally expanded CD4+ T cells. Real-time impedance measurements indicated increased cytotoxicity of mutated CD4 + T cells against the patient´s fibroblasts. High throughput drug-sensitivity testing suggested that mutations induce resistance to mTOR inhibitors but increase sensitivity for HSP90 inhibitors. Our findings suggest a novel explanation for the aberrant, persistent T cell activation in cGvHD, and pave the way for novel targeted therapies.

54 **INTRODUCTION**

55

56 Graft-versus host disease (GvHD) is the main complication of allogeneic hematopoietic stem cell
57 transplantation (allo-HSCT).(*1*) Chronic GvHD (cGvHD), that occurs more than 100 days after the
58 transplantation, develops in 30-70 % of allo-HSCT recipients. Affected patients frequently need
59 immunosuppressive treatment for years or even for a lifetime, and in many patients the condition is
60 fatal.(*2*) The genesis of cGvHD is multifactorial, but donor alloreactive lymphocytes are believed to be the
61 key pathogenetic drivers that target host tissues such as skin, soft tissues, oral mucosa, and eyes. In
62 particular, CD4+ T cells contribute to the early inflammation and tissue injury, to subsequent chronic
63 inflammation, and late aberrant tissue repair and fibrosis.(*3*)

64 During normal immune response, naïve T cells encounter their cognate antigen, get activated and
65 undergo a rapid clonal expansion.(*4*) The activation and proliferation of T cells are usually tightly regulated
66 processes, in which effector cells undergo apoptosis upon proper immune response. In many immune-
67 system-mediated disorders, such as cGvHD, the immune homeostasis is disturbed, and the enormous
68 variability of different T cell clones is diminished. In some patients, the T cell receptor (TCR) repertoire is
69 heavily skewed, and clones comprising up to 20-40% of all T cells can exist.(*5*) The underlying mechanisms
70 for this phenomenon remain unknown.

71 Here, we hypothesized that in cGvHD antigen-encountered T cells may acquire somatic mutations
72 due to constant immune-system activation and proliferation. Such mutations might lead to functional and
73 survival advantages of T cells that result in clonal expansion and aberrant immune responses. To explore
74 this theory, we sequenced purified CD4+ and CD8+ lymphocytes from an index patient suffering from
75 cGVHD with a custom deep-sequencing panel consisting of immunity and inflammation-related genes.
76 Mutation findings were confirmed in a validation cohort of 135 GVHD patients. Subsequently, the
77 functional consequences of the discovered mutations including their role in conferring resistance to

78 immunosuppressive therapy were evaluated *in vitro,* and finally verified with patient cells using drug

79 sensitivity screening and unbiased transcriptome-wide single-cell RNA-sequencing (scRNA-seq) paired with

80 T cell receptor alpha and beta sequencing (TCRab-seq) analysis and functional cytotoxicity assays.

81

RESULTS

Clinical Characteristics of the Index cGvHD Patient

The index patient was a 56-year-old male, who was diagnosed with chronic phase chronic myeloid leukemia in 1999. The clinical status and treatment history are described in detail in Supplemental Figure S1 and Supplemental results. Since the beginning of 2001, the patient suffered from cGvHD affecting his liver, eyes, nails, and skin. The immunosuppression was continuously adjusted according to the clinical presentation of the cGvHD.

Immunophenotype and clonal expansions of CD4+ and CD8+ T cells

During the first sampling in 2013, the patient was on mycophenolate mofetil therapy. T cell clonality was initially analyzed with a flow cytometry-based assay using a panel of TCR Vβ-specific antibodies. A large clonal Vβ20+ expansion was noted among CD4+ T cells. The Vβ20+ clone constituted approximately 50% of pure CD4+T cells and 60% CD4+CD8+ T cells (Figure 1A and 1B). Additionally, smaller clonal expansions (Vβ5.1 11.8%, Vβ7.1 21.0%, Vβ17 12.1%, and Vβ23 12.2%) were detected among CD8+ T cells (Figure 1B). To assess the clonality in more detail, FACS-sorted CD4+ Vβ20+, CD4+ Vβ20- and CD8+ T cells, obtained in 2015, were further analyzed by a TCRβ deep-sequencing assay(*6*), which confirmed the TCRBV30-01 clone expansion (corresponding to the Vβ20+ expansion observed by flow cytometry) in the CD4+Vβ20+ fraction (66.2% of sorted cells) (Figure 1C). TCRβ sequencing of CD8+ T cells revealed two relatively large clones, TCRBV07-09 (16.1%) and TCRBV28-01 (17.9%).

During an exacerbation of sclerodermatous skin lesions in 2015, 59% of peripheral blood leukocytes were T cells, 5% B cells, and 35% NK cells (Figure S2A in the Supplementary Appendix). CD3+ T cells were composed of CD4+ (47%), CD4+CD8+ (17%), and CD8+ T cells (27%) (Figure S2 in the Supplementary Appendix). An increased number of CD4+ effector memory (EM, 75.0%) and terminally differentiated effector memory (TEMRA) cells (17.4%) was found together with a decreased number of CD4+ central

106 memory (CM) cells (6.2%) when compared with the sibling donor's CD4+ T cell pool (59.6% EM, 5.0%
107 TEMRA, and 19.9% CM cells)(Figure 1D). In the CD8+ T cell pool, increased amount of TEMRA cells was
108 noted (79.9% of CD8+ T cells).
109
110 **Somatic Mutations in the Expanded CD4+ T Cell Population of the Index Patient**
111 To screen for somatic mutations, a customized immunity and inflammation-related gene sequencing panel
112 (immunogene panel)(*6*) was applied to immunomagnetic bead-separated blood CD4+ and CD8+ T cells, that
113 were obtained from the index patient in 2013. The median target gene coverage for the panel was 152 in
114 CD4+ and 160 for CD8+ T cells. In total, 14 candidate putative somatic mutations were discovered within
115 the CD4+ T cells (Table 1), and one in CD8+ cells (Table S7A in the Supplementary Appendix). Based on the
116 known biological significance, three of the mutations (*MTOR*, *NFkB2*, and *TLR2)* were considered as
117 putative driver mutations and potentially important for disease pathogenesis and were studied further.
118 The previously undescribed somatic missense mutation in *MTOR* (position 11182160, G to C) changes the
119 amino acid proline 2229 to arginine (Figure 2A). The variant allele frequency (VAF) was 13.3% among
120 CD4+T cells (Table 1). This mutation in exon 48 is located in the kinase domain which has been suggested to
121 be important for signal transduction.(*7*) In addition to *MTOR*, two other interesting mutations were
122 identified in the *NFkB2* and *TLR2* genes, although these were statistically not significant (p>0.01) due to the
123 low coverage in these locations (Table 1). The *NFkB2* missense mutation (position 104162075, C to A) leads
124 to a change of the amino acid proline 882 to glutamine (Figure 2A). *TLR2* missense mutation (position
125 154625732, G to T) results in a change of the amino acid tryptophan 558 to leucine (Figure 2A). The
126 transcription factor NFkB2 is a critical regulator of inflammation and immune function.(*8*) Toll-like-receptor
127 2 (TLR2) is one of the pattern recognition receptors and has been shown to be a crucial player for the
128 pathogenesis of autoimmune diseases. Notably, TLR2 protein has been shown to be highly expressed in
129 GvHD patients.(*9*)

130 As an additional confirmation of these findings, we performed exome sequencing of CD4+, CD8+ T cells,
131 and NK-cells obtained from the index patient in 2015 (Tables S7B, C, and D in the Supplementary
132 Appendix). Altogether, 15 candidate putative somatic mutations were discovered within the CD4+ T cell
133 population, including those in the *MTOR*, *TLR*2, and *NFkB2* genes (Table S7 in the Supplementary
134 Appendix).
135
136 **Validation of the MTOR, TLR2, and NFkB2 Mutations in the Index Patient**
137 To further validate the *MTOR P2229R*, *TLR2 W558L,* and *NFkB2 P882Q* mutations, CD4+ cells obtained in
138 2015 underwent standard capillary sequencing. Only the *MTOR* mutation was confirmed due to the low
139 sensitivity of the assay (Figure 2B). Therefore, targeted amplicon sequencing with a coverage up to
140 100.000X and a sensitivity of 0.5% VAF(*10*) was applied to all available samples from different time points
141 to establish the dynamics and the lineage specificity of the discovered mutations. The *MTOR* mutation was
142 detected in CD4+ T cells that were obtained in 2015 and 2017 with VAFs 19.2 % and 21.0 %, respectively
143 (Table 2 and Table S7 in the Supplementary Appendix). The VAF of the *MTOR* mutation appeared to
144 increase from 2013 to 2017 regardless of the continuous immunosuppressive therapy (Figure 2C). No
145 mutations or very low VAFs were detected within flow-sorted CD3-, CD8+/CD4-, CD4+Vβ20-, CD4+CD8+
146 Vβ20-, and monocyte samples (Figure S2C and Table S8 in the Supplementary Appendix). Thus, the
147 mutation was confined to the CD4+ Vβ20+ cell fraction (VAF 44.7% in flow-sorted cells).
148 Similarly, the *NFkB2 P882Q* mutation was confirmed to be limited to CD4+Vβ20+ T cells (VAFs: 12.0% in
149 CD4+ T cells and 21.3% in CD4+Vβ20+ cells) (Table 2, S7 and S8 in the Supplementary Appendix). In
150 contrast, *TLR2 W558L* mutation was discovered in both CD4+ (VAFs: 16.5% in CD4+ cells, 35.5% in
151 CD4+Vβ20+ cells) and CD8+ T cells (VAF 4.7 %) (Table S9 and S10 in Supplementary Appendix).
152

153 In the course of the disease, the cGvHD affected different organs of the index patient, but particularly the
154 skin. To explore whether lymphocytes harboring the detected somatic mutations can be found in target
155 organs, we screened paraffin-embedded biopsy samples by amplicon sequencing. The *MTOR* mutation was
156 identified in a sclerodermatous lesion that was biopsied in 2015 (VAF 0.8 %), but not in eye or liver biopsies
157 (Table 2). Immunofluorescence staining demonstrated CD4+ and CD8+ T cell infiltration in the same
158 sclerodermatous lesion (Figure 2D).
159 To examine whether the mutations were already present in the donor, both CD4+ and CD8+ T cells from
160 the donor were sequenced by amplicon sequencing, but no mutations were detected.
161
162 **Screening for the Identified *MTOR*, *TLR2,* and *NFkB2* Mutations in cGvHD patient Cohort**
163 To explore whether the found mutations are recurrent, blood samples from 135 cGvHD patients, 38 allo-
164 HSCT patients without cGvHD, and 54 healthy controls were screened by the amplicon sequencing. Two
165 additional cGvHD patients carried the same *MTOR* missense mutation yielding in a *MTOR P2229R* mutation
166 frequency of 2.2 % in all cGvHD patients (3 out of 135). In healthy controls or allo-HSCT patients without
167 cGvHD, no *MTOR* mutations were detected. Furthermore, *NFkB2* mutations were neither detected in
168 additional cGvHD patients nor in controls. The *TLR2 W558L* mutation was found in both cGvHD patients
169 and healthy controls, but the VAF indicated a 10- and 4-fold higher mutation frequency in cGvHD patients'
170 CD4+ and CD8+ T cells compared to healthy controls (Figure S3, Tables S9 and S10 in the Supplementary
171 Appendix).
172
173 **Identified Somatic Mutations Result in a Gain-of-function Alteration**
174 MTOR consists of two functionally distinct multi-protein complexes, mTORC1 and mTORC2. Eukaryotic
175 translation initiation factor 4E (eIF4E)-binding protein 1 (4E-BP1) and ribosomal S6 kinase (S6K1) are among
176 the key substrates of mTORC1, and as such critical regulators of cap-dependent translation.(*11*) mTORC2

177 directly phosphorylates AKT, thereby promoting cell survival.(*12*) Various genomic alterations have been
178 shown to aberrantly activate the mTOR pathways(*13*), which is marked by an increased phosphorylation of
179 downstream factors, such as S6K1, S6, and AKT. To examine the functional consequences of the *MTOR*
180 *P2229R* and other mutations, we transduced HEK293 human embryonic kidney cells with mutant
181 constructs. Both the *MTOR P2229R* single mutant and triple mutant resulted in a substantially enhanced
182 phosphorylation of S6K1, S6, and AKT compared to wild-type (WT) MTOR or triple WT (Figures 3A and B)
183 suggesting an activation of both mTORC1 and mTORC2 pathways.
184 The *NFkB2* P882Q mutation is located in the c-terminal domain (Figure 2A), which is known to play an
185 important role in the ubiquitination and partial proteolysis from NFkB2 (p100) to NFkB2 (p52).(*14*) In order
186 to determine the molecular balance between these two states, we performed immunoblotting which
187 revealed an increased expression of p52 (Figures 3C and D) indicating a gain-of-function alteration.
188 Similarly, to study the functional consequences of the *TLR2 W558L* mutation, we evaluated alterations in
189 transcriptional regulation by analyzing mRNA expression levels of a subset of *TLR2* downstream targets by
190 qRT-PCR. This demonstrated significantly increased expression levels of *ELK1* and *FOS1* in the *TLR2 W558L*
191 mutant expressing cell line as compared to the WT control (Figure S4B in the Supplementary Appendix).
192
193 **Paired scRNA- and TCRab sequencing of the CD4+ T cells from the index patient from two time points**
194 Recently, entire transcriptome at the single-cell level has been explosively studied for revealing a
195 differential gene expression profiles between individual cells, which cannot be identified from analysis of
196 mixed cells.(*15*)
197 In order to better understand the heterogeneity of the clonotype and the underlying CD4+ T cell
198 compartment in an unbiased manner, we performed simultaneous single-cell RNA and paired TCRab
199 sequencing on two time points in 2015 and 2017 for the index patient's CD4+ T lymphocytes from
200 peripheral blood. From the paired sequencing we received 15,847 CD4+ T lymphocytes passing the quality

201 control, and they could be divided into nine distinct phenotypes with graph-based clustering. Interestingly,
202 most of the cells (72.0%*)* were characterized by cytotoxicity (clusters 0, 1, 2 and 3), and lower frequency of
203 naïve cells (20.8%, clusters 4 and 5) and regulatory T cells (3.2%, cluster 8) were identified (Figure 4 A-C*).*
204 The frequency of cells in clusters were stable between the time points indicating resistance to the ongoing
205 immunosuppressive treatment, and only the two smallest populations showed over two-fold-change
206 between the two timepoints (clusters 3 and 7, Figure S5 in the Supplementary Appendix).
207 From the TCRab-seq we detected TCRab, TCRa or TCRb from 11,055 cells (71.4%), resulting in 3651 unique
208 T cell clonotypes. The clonotype matching to TCRVB sequencing data (Figure 1C) and harboring the *MTOR*-
209 mutation was also the most expanded fraction, representing 40.1% of the CD4+ T cells. Almost all of the
210 cells from this clonotype (90.1%) belonged to the cytotoxic clusters, and most of the cells were included in
211 the cluster 0 (74.6%) (Figure 4D).
212 To understand the effect of the *MTOR*-mutation on the T cells, we performed differential expression (DE)
213 analysis between the cytotoxic cells, comparing the cells from clonotype of interest against the other
214 cytotoxic cells in clusters 0, 1, 2 and 3. The analysis found 876 statistically significant DE-genes, of which
215 694 were upregulated in the clonotype, including cytotoxic genes (e.g. *GZMA*, *GZMAB, GNLY, GZMK*, *NKG7*
216 *and PRF1*), and HLA class I and II genes (Figure 4E). Additionally, upregulated eukaryote elongation factors
217 (*eEF*s), such as *EEF1A1, EEF1B2,* and *EEF2*, supported abnormal growth and proliferation of the expanded
218 CD4+ T cells. Furthermore, the expression of *DUSP2* and *KLRB1* genes was highly specific for the mutated
219 clone (Figure 4B). To identify differential pathway regulation in the clonotype, Gene Set Enrichment
220 Analysis (GSEA) was performed, resulting in 11 significantly over-represented and 0 under-represented
221 pathways in the clonotype (Table S11 in the Supplementary Appendix). The upregulated pathways included
222 *MTORC1*-pathway supporting the similar effect of the mutations in patient cells as observed in the *in vitro*
223 cell line models (Figure 4F). Other pathways found in the GSEA analyses included TNF-alpha signaling, IFNg
224 response and IL2-STAT5 signaling.

225 **Real-time cytotoxicity analysis of CD4+ T cells against primary fibroblasts from the index patient**

226 Real-time electrical impedance measurements monitoring target cell killing have been widely applied to
227 study the cellular cytotoxicity *in vitro*.(*16, 17*) To test the functional effects of the mutated CD4+ T cells and
228 to verify aberrantly upregulated gene expression signatures associated with cytotoxicity, we performed co-
229 culture experiments with CD4+ T cells and primary fibroblasts. Addition of purified CD4+ T cells on the
230 mono-layer of primary fibroblasts from the index patient resulted in decreased electrical impedance
231 implicating cytotoxicity of the CD4+ T cells (Figure 5A and B). In contrast, the CD8+ T cells showed no
232 cytotoxic activity against the fibroblasts, as the impedance curve mirrored the control well without effector
233 cells.

234

235 **Drug Sensitivity and Resistance Testing (DSRT) in CD4+ T cells from the Index Patient**

236 To determine sensitivity of the mutated cells to targeted therapy, robust *ex vivo* DSRT with 527 drugs in 5
237 different concentrations (*18*) was performed on freshly isolated CD4+ T cells from the index patient, the
238 donor, and a healthy control (Figure 6). In this screen, the index patient's CD4+ T cells were less sensitive to
239 mTOR/PI3K inhibitors as compared to the donor's CD4+ T cells (Figures 6A and B), although constitutive
240 PI3K/AKT/mTOR activity generally predicts rapalog sensitivity. Instead, we observed that heat shock
241 protein 90 (HSP90) inhibitors showed an increased killing effect on the index patient's CD4+ T cells as
242 compared to CD4+ T cells from the donor and healthy control (Figures 6A, C, and D). Interestingly, scRNA-
243 seq analysis indicated that one of HSP90 family members, HSP90AB1, was significantly upregulated in the
244 expanded CD4+ T cell clonotype, and it was one of the gene expression markers for the clonotype (Figure
245 4E). With regard to other clinically interesting drug classes, both the donor and the recipient CD4+ T cells
246 were sensitive to HDAC inhibitors, CDK-inhibitors, and proteosome inhibitors. The donor cells were also
247 modestly more sensitive to glucocorticoids (dexamethasone and methylprednisone), but this was not
248 statistically significant. Neither donor nor recipient CD4+ T cells were sensitive to cyclophosphamide,

249 tacrolimus, or methotrexate. However, it should be taken into account that the assay read-out is cell death,
250 and lymphocytes were not activated nor actively proliferating during the experiment.
251 In both WT and mutant HEK293 cells, the HSP90 inhibitor ganetespib reduced AKT phosphorylation on
252 serine 473. As expected, AKT-phosphorylation appeared to be normal following sirolimus treatment as
253 rapalogs only inhibit mTORC1 activity (Figures 6E and F). Treatment with either drug resulted in decreased
254 levels of phosphorylated S6K1 in both mutant and WT cells (Figure 6G). Both drugs also led to a reduced
255 pS6 phosphorylation in CD4+ T-lymphocytes from the index patient and a healthy control (Figures 6H and
256 I), suggesting an inhibitory effect on mTORC1 activity. Likewise, the scRNA-seq data analysis supported that
257 MTORC1 pathway is upregulated in the clonally expanded cytotoxic CD4+ T cells from the index patient
258 (Table S11 in the Supplementary Appendix). AKT was more phosphorylated in the patient's CD4+ T cells as
259 compared to controls with a slight decrease in both samples upon treatment with ganetespib or sirolimus.
260

261 **Discussion**

262 By analyzing blood CD4+ and CD8+ T cells we discovered a recurrent somatic missense mutation in
263 *MTOR* in cGvHD patients. In the index patient, the mutation was limited to the expanded CD4+ T cell clone,
264 it persisted for years and was found in both blood and sclerodermatous skin lesion samples. Paired scRNA-
265 and TCRab-seq verified that the majority of the expanded CD4+ T cells had upregulated expression of genes
266 associated with cytotoxicity and cellular proliferation. Furthermore, mutated CD4+ T cells possessed
267 cytotoxicity against patient's own primary fibroblasts. No mutations were discovered in the sibling donor
268 samples suggesting the mutations been formed after the allo-HSCT. Functional *in-vitro* studies indicate that
269 the *MTOR* mutation results in a gain-of-function alteration activating both mTORC1 and mTORC2 pathways.
270 Accumulation of somatic mutations is inherently associated with normal cell division. The role of
271 somatic mutations in cancer is well established, and interestingly, recent reports suggest that somatic
272 mutations may also play a role in the pathogenesis of non-malignant diseases.(*19-23*) We have previously

273 shown that somatic mutations occur in cytotoxic lymphocytes of newly diagnosed rheumatoid arthritis
274 patients(*6*) and in patients with large granular lymphocytic proliferation.(*24*) Interestingly, it was also
275 recently shown, that the disruption of the *TET2* gene by lentiviral vector-mediated insertion of the chimeric
276 antigen receptor (CAR) transgene led to the expansion of single CAR T cell in a patient with chronic
277 lymphocyte leukemia and enhanced therapeutic efficacy.(*25*) In addition to lymphoid cell-related disorders,
278 recent studies have suggested that somatic mutations may play a role in the pathogenesis of other non-
279 cancerous diseases such as *KRAS* mutations in brain arteriovenous malformations leading to activation of
280 the MAPK-ERK pathway.(*23*)

281 The novel *MTOR P2229R* kinase domain mutation discovered in our cohort has not been previously
282 reported, although already over 750 different *MTOR* mutations exist in the COSMIC database. Previously,
283 mutations in the same domain have been shown to lead to the activation of the mTORC1. The
284 PI3K/AKT/mTOR axis controls important cellular processes and is frequently dysregulated in various cancer
285 types.(*26*) This pathway is also important for the regulation of T cell activation, function, and survival.(*27*)
286 Inhibition of the PI3K/AKT/mTOR axis by targeting the mTORC1 complex with rapamycin has been used to
287 prevent and treat GvHD.(*28*) Based on our data, the *MTOR P2229R* mutation induces the activation of both
288 the mTORC1 and mTORC2 as noted by increased S6K and AKT phosphorylation. Additionally, scRNA-seq
289 analysis strongly supported that *MTORC1* pathway is upregulated in the clonally expanded and cytotoxic
290 CD4+ T cells from the index patient.

291 In addition to *MTOR*, the mutation in the *NFKB2* gene is also a putative driver due to the
292 importance of this signaling pathway in the immune system. NF-κB has been extensively described as one
293 of the main regulators of the inflammatory response and cancer pathogenesis, offering a promising target
294 in anti-inflammation and -cancer drug development.(*29*) Both p50/RelA-mediated canonical and p52/RelB-
295 mediated non-canonical pathways are involved in NFκB activation. Phosphorylated NFκB2 (p100) is
296 associated with RelB and sequentially ubiquitinated at the C-terminus to form the p52/RelB complex,

297 which is translocating into nucleus and activating downstream target genes.(*30*) Therefore, p52 formation
298 in NFκB2 (p100) processing is a key step for the activation of the non-canonical NFκB pathway. Especially
299 two serine residues in the C-terminal domain of NFκB2 (p100), S866 and S870, are necessary for NFκB2
300 (p100) processing.(*31*) The index patient harbored *NFkB2* (p100) *P882Q* somatic mutation located in the C-
301 terminus, which has not been reported in the COSMIC before. This mutation leads to an increased p52
302 formation which potentially induces a hyper-activation of non-canonical NF-κB pathway contributing to
303 chronic inflammation in the index patient.

304 Unlike the discovered *NFkB2* and *MTOR* mutations, the *TLR2 W558L* somatic mutation was
305 identified in both cGvHD patients and healthy controls. However, VAFs were significantly higher in cGvHD
306 patients as in healthy controls. TLR2 is one of the pathogen-associated molecular pattern recognition
307 receptors and regulators of innate immunity, and it is constitutively expressed on regulatory and memory
308 CD4+ T cells.(*32*) TCR activation by an anti-CD3 antibody has been shown to induce the overexpression of
309 TLR2 on naïve CD4+ T cells followed by activation of the MyD88-dependent *NF-κB* signaling cascade and
310 inflammatory gene expression in peripheral blood.(*33*) Thus, in combination with the *NFkB2* and *MTOR*
311 mutations, the *TLR2 W558L* mutation may further enhance the activation of the *NF-κB* and inflammatory
312 pathways.

313 Single-cell RNA-seq analysis revealed that the clonally expanded CD4+ T cells had upregulated
314 gene expression signatures associated with cytotoxicity (*GZMA*, *GZMB*, *GNLY* and *NKG7)* and proliferation
315 (*DUSP2*, *KLRB1*, *EEF1A1*, *EEF1B2*, and *EEF2*). Furthermore, real-time impedance analysis indicated
316 cytotoxicity of CD4+ T cells from the index patient, whereas the CD8+ T cells had no effect. Although
317 cytotoxicity has not been considered as a typical CD4+ T cell function (*34*), cytotoxic potential of T helper
318 cells (CD4+CTL) has been recently described including a granzyme-mediated killing capability of target cells
319 during viral infections.(*35, 36*) Epigenetic and molecular mechanisms leading into CD4+CTL differentiation
320 has not yet been clearly described.(*37*) From the proliferation associated genes, DUSP2 (PAC-1) was one of

321 the hallmark genes associated with the mutated clonotype. It is known as one of the MAPK phosphatases,
322 which play an important role in deactivating MAPK. DUSP2 is shown to be up-regulated in T cell activation
323 associated with inflammation.(*38*) Murine knockout phenotype studies for DUSP2 presented reduced
324 cytokine production and protected from inflammatory arthritis. In the murine colitis model, DUSP2
325 knockout induced Th17 differentiation by directly enhancing the transcriptional activity of STAT3.
326 Therefore, DUSP2 inhibit Th17 lineage of T cell development by attenuated STAT3 activity through
327 dephosphorylation of STAT3 at Tyr705 and Ser727.(*39*) In addition, it has been indicated that DUSP2 inhibit
328 JNK leading to ERK pathway activation.(*40*) Interestingly, TLR2 stimulation also strongly correlate with ERK
329 activation. ERK(1/2) pathway is well known for a positive selection of T cell development and proliferation,
330 and especially CD4+ T cell differentiation depends on ERK signaling.(*41*) Taken together, DUSP2 up-
331 regulation in scRNA seq data support the expansion of CD4+T cells in the index cGVHD patient.
332 Drug sensitivity testing with patient cells indicated a lower efficacy of mTOR/PI3K inhibitors
333 compared to the donor, suggesting a hyperactivation of mTOR pathway due to the mutation. However, the
334 effect of ongoing immunosuppressive treatment (mycophenolate) cannot be ruled out as it may also affect
335 mTOR signaling.(*42*) Since the mTOR pathway is hyperactivated in many different types of cancer and
336 autoimmune diseases, mTOR inhibitors have been developed and applied to prevent dysregulated mTOR
337 signaling.(*43-46*) Rapamycin and its analogs are highly specific mTOR inhibitors that form a complex with
338 FKBP2, which selectively binds to the FRB domain of mTOR, leading to targeted inhibition of mTORC1-
339 mediated signaling pathways. Therefore, alternative therapeutic applications have been suggested for
340 additionally targeting the dysregulated mTORC2 signaling pathway. Initially, Zheng et al. indicated that the
341 kinase domain of mTOR is a more potent site for mTOR inhibition as it is necessary for both rapamycin-
342 insensitive and rapamycin-sensitive aspects of cell growth and survival.(*47*) ATP-competitive mTOR
343 inhibitors targeting the kinase domain of mTOR have already been developed to inhibit both mTORC1 and

344 mTORC2-mediated signaling processes.(*48, 49*) These inhibitors demonstrated a better clinical efficacy and
345 lower toxicity in anti-tumor therapy as compared with rapalogs.(*7*)
346 Interestingly, HSP90 inhibitors showed higher efficacy when compared to mTOR inhibitors in the
347 DSRT assay. HSP90 is one of the most abundant and conserved ATP-dependent molecular chaperons,
348 whose expression increases by up to 10-fold under physiologic stress conditions.(*50*) Functionally, HSP90
349 plays an important role in the refolding of denatured proteins under stress conditions.(*51, 52*) In addition,
350 it activates these proteins including growth-stimulating proteins and kinases.(*50*) mTOR, through its
351 mTORC1 component raptor, directly binds to HSP90 in primary T cells in order to regulate mTOR signaling
352 processes.(*53*) Additionally, AKT physiologically interacts with HSP90 to activate mTOR pathway
353 signaling.(*54*) Notably, HSP90 overexpression has been suggested to be correlated with Akt/mTOR pathway
354 activation in cancer. Furthermore, HSP90 inhibitors have been shown to suppress the Akt/mTOR pathway
355 activity.(*55*) Therefore, HSP90 has become a therapeutic target for several cancer types, and many HSP90
356 inhibitors are under the evaluation in phase I and II clinical trials for cancer therapy.(*56*) Importantly, HSP90
357 inhibitors have also been suggested to have protective and therapeutic effects in mouse models of
358 GvHD.(*57*) To our knowledge, these have not yet been used to treat GvHD patients, but based on our
359 results HSP90 inhibitors could serve as a novel therapeutic approach in a subset of cGvHD patients.
360 In conclusion, novel *MTOR, NFkB2,* and *TLR2* somatic mutations were discovered in an expanded
361 CD4+ T cell clone in a patient with cGvHD. The mutations persisted over time and induced activation of the
362 *NF-kB* and *MTOR* pathways. The *MTOR* mutation was found to be recurrent in other cGvHD patients.
363 Although the *MTOR* mutation frequency was low in the total cGvHD cohort, somatic mutations may also
364 exist in other genes, and similar small subgroups of cGvHD patients can be discovered warranting further
365 investigations. Our findings imply a novel mechanism for the aberrant, persistent T cell activation in cGvHD
366 and pave the way for potential novel individualized therapies.
367

368 **MATERIALS AND METHODS**
369
370

371 **Study Patients**

372 Samples were collected between 2007-2016 from 135 patients who had developed cGvHD after allo-HSCT
373 (Helsinki University Hospital, Helsinki, Finland, n=8; Turku University Hospital, Turku, Finland, n=37;
374 Hospital de la Princesa, Madrid, Spain, n=19; Hospital Morales Meseguer, Murcia, Spain, n=71). In addition,
375 38 patients who had not developed cGvHD until the date of sampling, served as a control cohort (Turku
376 University Hospital n=6 and Hospital Morales Meseguer n=32). The blood samples were collected 3 to 102
377 months (mean 13.5 months) and 2 to 47 months (mean 14.5 months) after allo-HSCT for GvHD and non-
378 cGvHD patients, respectively. Clinical characteristics of the patients are summarized in Supplemental Table
379 S1. All patients provided written informed consents. Additionally, buffy coat samples from 54 healthy blood
380 donors were obtained from the Finnish Red Cross Blood Service. A peripheral blood sample from the index
381 patient's sibling donor was also obtained.
382 The study was performed in compliance with the principles of Helsinki declaration, and was approved by
383 the ethics committees in the Helsinki University Hospital (Helsinki, Finland), Turku University Hospital
384 (Turku, Finland), Hospital de la Princesa (Madrid, Spain) and Hospital Morales Meseguer (Murcia, Spain).
385

386 **Reagents**

387 Primary antibodies against NFkB2 (Cat#: 4882S, Lot: 4), ribosomal protein S6 (Clone: 54D2, Cat#: 2317S,
388 Lot#: 4), phospho-S6 ribosomal protein (Ser235/236) (Clone: D57.2.2E, Cat#: 4858T, Lot#: 16), Akt (Clone:
389 C67E7, Cat#: 4691T, Lot#: 20), phospho-Akt (Ser473) (Cat#: 9271T, Lot#: 14), p70S6 kinase (S6K) (Clone:
390 49D7, Cat#: 2708T, Lot#: 7), and phospho-p70S6 (S6K) kinase (Thr421/Ser424) (Cat#: 9204S, Lot#: 11) were
391 purchased from Cell Signaling Technology, and antibody against beta-actin (Clone: AC15, Cat#: ab6276,

392 Lot#: GR66278-11) was purchased from Abcam. Secondary antibodies, IRDye 700 conjugated anti-mouse
393 and IRDye 800 conjugated anti-rabbit, were purchased from LI-COR Biosciences.
394
395 **Cell Lines**
396 Human embryonic kidney HEK293 cells (Cat#: CRL-1573, ATCC) and HEK293FT (Cat#:R70007, Thermo Fisher
397 Scientific) were maintained in high-glucose Dulbecco Modified Eagle medium (Lonza) containing 10% FBS
398 (Gibco), 1% penicillin-streptomycin (Invitrogen), and L-glutamine (Lonza) in a 37 °C humidified incubator
399 with 5% CO2. Cell line authentication was performed with GenePrint10 System (Promega). HEK293 cell line
400 was authenticated *via* Promega GenePrint10 System. The result was compared ATCC STR, JCRB STR, ICLC
401 STR database, and DSMZ online STR database. The identity estimates are calculated according to the allele
402 information found in these databases. HEK293FT cell line was derived from Thermo Fisher Scientific with
403 an authentication and only less than 10 passages were used. Mycoplasma test was performed using
404 MycoAlert Mycoplasma Detection Kit (LONZA, Cat#: LT07-318).
405
406 **Sample Preparation and DNA Extraction**
407 Mononuclear cells (MNCs) were separated from whole blood using Ficoll-Paque™ PLUS (GE Healthcare).
408 The separated MNCs were then labeled with either CD4+ or CD8+ magnetic beads (Miltenyi Biotec) and
409 sorted by AutoMACs® cell sorter (Miltenyi Biotec) according to the manufacturer's protocol. The purity of
410 sorted fractions was evaluated by flow cytometry and confirmed to be >98% (FACsVerse, BD Biosciences).
411 Alternatively, separated MNCs were sorted using FACsAria II (BD Biosciences). Genomic DNA was isolated
412 from fresh or frozen sorted MNCs or from whole blood samples using the Genomic DNA NucleoSpin Tissue
413 kit (Macherey-Nagel). DNA concentration and purity were measured with Qubit2.0 Fluorometer (Invitrogen)
414 or Nanodrop (Thermo Fisher Scientific).
415

416 **Flow Cytometry Analysis and Flow-assisted Cell Sorting**

417 For phenotyping of the memory T cell subsets, peripheral blood mononuclear cells (PBMCs) were
418 immunostained with the antibody panel including anti-CD3 PeCy7 (Clone: SK7, Cat#: 557851, Lot#:
419 8037645, BD Biosciences), -CD4 PerCP (Clone: SK3, Cat#: 345770, Lot#: 6281605, BD Biosciences), -CD8
420 PerCP (Clone: SK1, Cat#: 345774, Lot#: 82152, BD Biosciences) -CD45RA Alexa700 (Clone: HI100, Cat#:
421 560673, Lot#: 7180940, BD Biosciences), and -CCR7 PE (Clone: 150503, Cat#: FAB197P, Lot#: LEU1618031,
422 R&D System). Stained samples were analyzed with FACSVerse (BD Biosciences) and FlowJo software
423 (Version 10.4.2). For CD4+ T cell TCR Vβ20+ clone sorting, PBMCs were immunostained with anti-CD3 APC
424 (Clone: SK7, Cat#: 345767, Lot#: 7236657, BD Biosciences), -CD4 PerCP (Clone: SK3, Cat#: 345770, Lot#:
425 6281605, BD Biosciences), -CD8 PE-Cy7 (Clone: SK1, Cat#: 335822, Lot#: 8272690, BD Biosciences) and -
426 Vβ20 (IOTest® Beta Mark TCR Vbeta Repertoire Kit, Cat#: IM3497, Lot#: 66, Beckman Coulter). Stained cells
427 were physically isolated by FACs AriaIII (BD Biosciences) and analyzed with FlowJo software. Purity of
428 sorted cells was more than 99% and verified with the same system. (Supplementary Figure S2C)
429

430 **TCR Vβ Analysis**

431 TCR Vβ families were analyzed from peripheral whole-blood samples by flow cytometry based antibody
432 staining using IOTest® Beta Mark TCR Vβ Repertoire Kit (Cat#: IM3497, Lot#: 66, Beckman Coulter). Briefly,
433 CD4+ and CD8+ T cells in whole blood samples were stained with the panel of TCR Vβ antibodies
434 recognizing 24 members of TCR β chain, which covers about 70% of the normal human TCR Vβ repertoire.
435 Stained cells were further analyzed using FACSVerse (BD Biosciences).
436
437
438 **TCR CDR3 Deep Sequencing**
439
440 Isolated genomic DNAs was used for TCRB deep sequencing. Sequencing and data analysis was conducted
441 with ImmunoSEQ assay as previously described (Adaptive Biotechnologies, Seattle, WA).(*58*)

442

443 **Immunopanel Sequencing**

444 A customized NGS panel including exonic areas of 986 genes related to immunity and cancer was used to
445 screen for somatic mutations.(*6*) Genes included in the panel are provided in the Supplemental Table S2.
446 Sequencing was done from both sorted CD4+ and CD8+ T cells. Bioinformatic analysis to identify and
447 annotate somatic variants was performed as previously described.(*6, 24*)

448

449 **Validation of the Somatic MTOR Mutation by Capillary Sequencing Analysis**

450 A specific primer set was designed using the Primer-Blast search (National Center for Biotechnology
451 Information: http://blast.ncbi.nlm.nih.gov/) to validate the somatic MTOR mutation (Supplementary Table
452 S3). Polymerase chain reaction (PCR) products were purified with the ExoSAP-IT (Affymetrix) followed by
453 sequencing on DNA sequencer (Applied Biosystems). Sequences were analyzed using 4Peaks version 1.7.1.

454

455 **Amplicon Sequencing of MTOR, NFkB2 and TLR2**

456 Targeted amplicon sequencing was performed with an in-house developed deep amplicon sequencing
457 panel using the Illumina Miseq platform (Supplementary Table S4). The coverage was over 100,000 X, and a
458 variant was called if variant base frequency was 0.5% of all reads covering a given a position. All variants
459 with the base quality frequency ratio (ratio of number of variant calls/ number of all bases and quality sum
460 of variant calls / quality sum of all bases at the position) ≥ 0.9 were considered as true somatic variants. A
461 detailed sequencing protocol and the bioinformatics pipeline used for data analysis are described in
462 previous reports.(*6, 24*)

463

464 **scRNA-seq and TCRab-seq analysis**

465 CD4+ T cells from two time points of the index patient were enriched using CD4 microbeads (Miltenyi
466 Biotec). Single cells were partitioned using a Chromium Controller (10x Genomics) and scRNA-seq and
467 TCRab-libraries were prepared using Chromium Single Cell 5' Library & Gel Bead Kit (10x Genomics), as per
468 manufacturer's instructions (CG000086 Rev D). In brief, 17,000 cells from each sample, suspended in 0.04%
469 BSA in PBS were loaded on the Chromium Single Cell A Chip. During the run, single-cell barcoded cDNA is
470 generated in nanodroplet partitions. The droplets are subsequently reversed and the remaining steps are
471 performed in bulk. Full length cDNA was amplified using 14 cycles of PCR (Veriti, Applied Biosystems). TCR
472 cDNA was further amplified in a hemi-nested PCR reaction using Chromium Single Cell Human T Cell V(D)J
473 Enrichment Kit (10x Genomics). Finally, the total cDNA and the TCR-enriched cDNA was subjected to
474 fragmentation, end repair and A-tailing, adaptor ligation, and sample index PCR (14 and 9 cycles,
475 respectively). The gene expression libraries were sequenced using an Illumina NovaSeq, S1 flowcell with
476 the following read length configuration: Read1=26, i7=8, i5=0, Read2=91. The TCR-enriched libraries were
477 sequenced using an Illumina HiSeq2500 in Rapid Run mode with the following read length configuration:
478 Read1=150, i7=8, i5=0, Read2=150. The raw data was processed using Cell Ranger 2.1.1. with GRCh38 as
479 the reference genome.
480 During secondary analysis, cells with fewer than 200 or more than 4000 genes, or more than 15% of the
481 counts from mitochondrially-encoded transcripts were excluded from the analysis. The remaining data was
482 log-normalized and scaled. To reduce the dimensionality of the data, we determined the highly variable
483 genes as the genes with the highest variance-mean ratio. Genes that had mean expression between 0.0125
484 and 3 on a log-transformed count scale and genes above 0.5 log(variance/mean) were counted as highly
485 variable, resulting in 764 genes. The T-cell receptor V-genes, mitochondrial genes and ribosomal genes (n =
486 113) were excluded from the results, resulting in a final list of 651 highly variable genes.
487 Clusters were identified using the graph-based community identification algorithm as implemented in the
488 Seurat-package(*28*). Prior to calculating cell-cell distances, PCA was performed on the 651 highly variable

489 genes on all the QC-positive cells, and the top 50 principal components were kept. To prevent
490 overclustering, the optimal number of clusters was determined by increasing the resolution
491 hyperparameter as a function of number of clusters until the first saturation plateau was achieved. The
492 robustness of these clusters was assessed by subsampling cells and doing the analysis iteratively and
493 visually inspecting the results of embedding and differentially expressed genes between the formed
494 clusters. Differential expression analysis was performed based on the t-test, as suggested by Robinson et
495 al(*59*). Clusters were annotated using canonical cell type markers as well as the differentially expressed
496 genes.
497 Gene Set Enrichment Analysis (GSEA) (software.broadinstitute.org/gsea/index.jsp) between the clonotype
498 and other cytotoxic cells was performed on genes that were detected at least in 0.1% of the cytotoxic cells
499 and had at least log fold-change of 0.01 between the clonotype and other cytotoxic CD4+ T cells. The gene
500 list was ordered based on the fold-change. Overlap with HALLMARK-category was assessed and the False
501 Discovery Rate (FDR) calculated while the number of permutations was 1000.
502 Clonotypes were identified based on the available information, and both total nucleotide level TCRa and
503 TCRb were used if found. Cells for which more than two recombinants were identified were excluded from
504 further analysis.
505 From the TCRab-seq we detected TCRab, TCRa or TCRb from 11,055 cells (71.38%), resulting in 3651
506 different T cell clonotypes. The clonotype harboring the *MTOR*-mutation was the most expanded,
507 compromising of 2366 cells (TRA:CLVGDIGNQGGKLIF; TRB:CAWSTGQANNSPLHF). However, we noticed that
508 the second most (TRB:CAWSTGQANNSPLHF, 1545 cells) and third most expanded (TRA:CLVGDIGNQGGKLIF,
509 598 cells) clonotypes had only one chain and as they matched to the most expanded clonotype, we treated
510 this as error coming from uncomplete sequencing and pooled the three most expanded clonotypes into
511 one.
512

513 **Analysis of cellular cytotoxicity**

514 Primary fibroblasts from the index patient were cultured based on previous method.(*60*) Briefly, skin
515 biopsy from the index patient were dissected in small pieces (approx. 2mm x 2mm) and transferred into 6-
516 well plate in 500 µl of complete growth medium containing 20% FBS. 2-300µl of growth medium was
517 added for every 2 days to replace evaporated media. After one week, increase amount of media to 2 ml
518 and change the media every 3 days. Once cells were confluent in each well, cells were trypsinized and
519 passaged.

520 To measure cellular cytotoxicity of CD4+ and CD8+ T cells from the index patient, the proliferation of the
521 fibroblast established from the index patient was monitored with xCELLigence™ real-time cell analyzer
522 (RTCA) (ACEA Biosciences, CA, USA) according to the manufacture's instruction. xCELLigence™ RTCA
523 biosensor measures cellular adhesion through electrical impedance, which is converted to Cell Index
524 (arbitrary units). Briefly, the E-Plate 16 VIEW (ACEA Biosciences, CA, USA) was equilibrated with the 100 µl
525 of culture media at room temperature. 100 µl of the cell suspension (8 x 10^3 cells/well) in duplicate was
526 transferred to the plate followed by incubation at room temperature for 30 min to allow the cells to settle
527 at the bottom of the wells. The xCELLigenceTM monitored the cells every 30 min for 200 repetitions. When
528 the cell index [(impedance at time point n – impedance in the absence of cells)/nominal impedance value]
529 were reached a plateau, CD4+ T cells, CD8+ T cells, and NK92 as an cellular cytotoxicity inducer (6.4 x 10^4
530 cells as a ratio of the fibroblast to the inducer is 1:8) for the fibroblast were added on the plate. CD4+ T
531 cells and CD8+ T cells were separated from MNCs with CD4+ or CD8+ magnetic beads (Miltenyi Biotec) and
532 sorted by AutoMACs® cell sorter (Miltenyi Biotec) according to the manufacturer's protocol. The real-time
533 impedance trace for the fibroblasts exposed to CD4+ T cells, CD8+ T cells, and NK-92 were monitored for 48
534 h.

535

536 **Multiplexed Immunohistochemistry (mIHC)**

537 Tissue blocks were cut in 3.5 µm sections. Slides were deparaffinized in xylene and rehydrated in graded
538 ethanol series and H2O. Heat-induced epitope retrieval (HIER) was carried out in 10 mM Tris-HCl - 1 mM
539 EDTA buffer in +99°C for 20 min (PT Module, Thermo Fisher Scientific). Peroxide activity was blocked in 0.9%
540 H2O2 solution for 15 min, and protein block performed with 10% normal goat serum (TBS-NGS) for 15 min.
541 Anti-CD3 (Clone: EP449E, Cat#: ab52959, Lot#: GR140731, Abcam) primary antibody diluted 1:500 in
542 protein blocking solution and secondary anti-rabbit horseradish peroxidase-conjugated (HRP) antibodies
543 (Immunologic) diluted 1:1 in washing buffer were applied for 1h45min and 45 min, respectively. Tyramide
544 signal amplification (TSA) 488 (PerkinElmer) was applied on the slides for 10 min. Thereafter, HIER,
545 peroxide and protein block were repeated, followed by application of anti-CD8 (1:500, Clone: C8/144B,
546 Cat#: BSB 5174, Lot#: 5174JDL05, BioSB) primary antibody, HRP-conjugated secondary antibody diluted 1:3
547 with washing buffer and TSA 555 (PerkinElmer). HIER, peroxide block and protein block were repeated.
548 Then, the slides were incubated with CD4 primary antibodies (1:25, Clone: EPR6885, Cat#: ab133616, Lot#:
549 GR218457, Abcam) overnight in +4°C. Next, AlexaFluor647 fluorochrome-conjugated secondary antibody
550 (Thermo Fisher Scientific) diluted in 1:150 and Dapi (Roche) counterstain diluted 1:250 in washing buffer
551 were applied for 45 min. ProLong Gold mountant (Thermo Fisher Scientific) and a coverslip were applied on
552 the slides. After peroxide block, antibody incubations and fluorochrome reaction, slides were washed three
553 times with 0.1% Tween-20 (Thermo Fisher Scientific) diluted in 10 mM Tris-HCL buffered saline pH 7.4 (TBS).
554 Fluorescent images were acquired with the AxioImager.Z2 (Zeiss) microscope equipped with a Zeiss Plan-
555 Apochromat 20x objective.
556
557 **Site-Directed Mutagenesis**
558 Site-directed mutagenesis was conducted using GENEART® Site-Directed mutagenesis system according to
559 the manufacturer's instruction (Invitrogen) with NFkB2 (GeneCopoeia, Cat.No. EX-Z4293-Lv154), TLR2

560 (GeneCopoeia, Cat.No. EX-Q0161-Lv122, GeneCopoeia), and mTOR (Addgene, Cat.No.26603) expression
561 vector. The primer sequences used for the site-directed mutagenesis are in the Supplemental Table S5.
562
563 **Establishing Stable Cell Lines**
564 HEK293 cells were transfected using FuGENE HD transfection reagent (Promega) with either a wildtype or
565 P2229R *MTOR* expression vector (ratio of reagent to DNA is 3:1) following the manufacturer's instruction.
566 Neomycin resistant clones were selected after the cells were cultured with G418 (500 µg/mL) for 3 weeks.
567 The lentiviruses were produced by co-transfection of HEK293FT cells with *NFkB2* (wildtype or P882Q
568 mutant) or *TLR2* (wildtype or W558L mutant) lentiviral expression vectors, and psPAX2 lentiviral packaging
569 plasmid (Addgene) and pCMV-VSV-G envelope plasmid (Addgene) using Lipofectamine® 2000 (Thermo
570 Fisher Scientific). Antibiotic free DMEM containing 10% FBS was used as a culturing medium and Opti-MEM
571 I Reduced Serum Medium (Thermo Fisher Scientific) supplemented with 5% FBS and 1 mM Sodium
572 pyruvate was used as a lentivirus packaging medium. 6 hours post-transfection, medium was removed and
573 replaced with DMEM. After 48 hours, the supernatants were centrifuged at 300 g for 5 min to remove cell
574 debris and filtered with a 0.45 µm polyethersulfone membrane filter. Ultracentrifugation to concentrate
575 the virus was performed for 2 hours at 12,000 g and 4°C using Beckman SW28 rotor. Lentivirus titers were
576 measured by p24 specific enzyme-linked immunosorbent assay.
577
578 **Establishment of Triple Mutant Stable Cell Lines**
579 HEK293 cells stably expressing exogenous *MTOR* (wildtype or P2229R mutant) were transduced with NFkB2
580 (wild type or P882Q mutant) expressing lentiviruses. Infections were performed in the presence of 8 µg
581 /mL of polybrene under centrifugation (500 g, 37°C) for 2 hours. *MTOR-NFkB2* transduced cells (expressing
582 Cyan Fluorescent Protein) were selected by using FACsAriaIII (BD Biosciences). Cells expressing exogenous

583 *MTOR-NFkB2* (wildtype or mutant) were infected with *TLR2* (wildtype or W558L mutant) expressing
584 lentiviruses as described above and selected using puromycin (3 µg/mL).
585
586 **Western Blot Analysis**
587 After removing serum containing medium, HEK293 cells were washed twice with ice-cold PBS followed by
588 serum starvation for 12 hours. Cells were then harvested and further lysed in ice-cold RIPA buffer with 1X
589 protease and phosphatase inhibitor cocktail (Thermo Fisher Scientific). To remove cell debris,
590 centrifugation was carried out for 10 min at 4 °C, 12,000 g. Total protein concentration was measured with
591 the Qubit protein assay (Thermo Fisher Scientific) and 5 µg of protein per sample was prepared in Laemmil
592 buffer (Bio-Rad Laboratories) to load on a SDS-PAGE gel (Bio-Rad Laboratories). After running the sample in
593 the SDS-PAGE gel, the proteins were transferred into a nitrocellulose membrane (Merk Millipore) followed
594 by blocking the membrane with Odyssey blocking buffer (LI-COR Biosciences) for 1 hour. Primary
595 antibodies (1:1000 dilution) were incubated overnight at 4°C in PBS with 0.1% Tween 20 containing 5% milk,
596 and subsequently secondary antibodies (1:15,000 dilution) in PBS with 0.1% Tween 20 containing 5% milk
597 were incubated for 1 hour at room temperature. The proteins were visualized using Odyssey Imaging
598 Systems (LI-COR Biosciences).
599
600 **Drug Sensitivity and Resistance Testing (DSRT)**
601 *Ex-vivo* DSRT was performed on freshly isolated CD4+ T cells with a total of 527 drugs in 5 concentrations
602 covering a 10,000-fold concentration range including conventional chemotherapeutics and a broad range
603 of targeted oncology compounds.(*47*) To dissolve the drug compounds, 5 µl of medium was dispensed into
604 each well of 384 well plates including five different concentrations of each drug. 20 µl of cell suspension
605 (CD4+ T cells from healthy control, donor and index patient: 2,000 cells per well) was transferred to every
606 well using MultiFlo FX dispenser (BioTek). After incubation (5% CO2 at 37°C) for 72 hours, the cell viability

607 was evaluated by CellTiter-Glo Assay solution (Promega). The drug sensitivity score (DSS) was calculated to
608 evaluate quantitative drug profiles based on the measured dose-response curve.(*61*)
609
610
611 **Reverse Transcriptase-quantitative Polymerase Chain Reaction (RT-qPCR)**
612
613 Total RNA was extracted using the RNeasy Mini kit (Qiagen) followed by cDNA synthesis using QuantiNova
614 Reverse Transcription kit (Qiagen) according to the manufacturer's protocol. The cDNA was applied in SYBR
615 Green RT-PCR master mix (Applied Biosystems) and oligonucleotide primers (Supplementary Table S6). All
616 RT-qPCR reactions were performed in 384-microwell plates (Applied Biosystem) using a QuantStudio 6 Flex
617 Real-Time PCR system (Applied Biosystems). The relative quantitation of gene expression was analyzed
618 using comparative cycle threshold (ΔΔCT) method, and beta actin (ACTB) was used as an endogenous
619 control to normalize gene expression level.
620
621 **Data availability**
622 Patient whole-exome and RNA-sequencing raw data related to table 1 and figure 4 are available from the
623 corresponding author upon request owing to regulations pertaining to the authors ethics permit and
624 deposition of these data in public repositories.
625
626 **Statistical Analysis**
627 Unpaired two-sided t-tests were performed using GraphPad Prism 6 for Mac OS X, version 6.0. In all
628 analyses, P-value < 0.05 was considered as statistically significant.
629
630

631 **List of Supplementary Materials:**

632 Supplementary results: Clinical Characteristics of the Index cGvHD Patient

633 Supplementary Figure S1. Medical history of the index patient

634 Supplementary Figure S2. Flow cytometry analysis of the index patient

635 Supplementary Figure S3. Variant allele frequencies of TLR2 mutations in cGVHD patients' and healthy

636 controls' CD4+ and CD8+ T cells

637 Supplementary Figure S4. Functional analysis of wild type and TLR2 mutants in HEK293 cell line

638

639 Supplementary Figure S5. Gene expression fold change within CD4+ cell clusters between 2015 and 2017.

640

641 Supplementary Table S1. Summary of study cohorts

642 Supplementary Table S2. Gene list in the immunogene panel sequencing.

643 Supplementary Table S3. Primer sets of mTOR, NFkB2 and TLR2 amplicon sequencing

644 Supplementary Table S4. Primer set for mTOR, NFkB2 and TLR2 capillary sequencing

645 Supplementary Table S5. List of mTOR, NFkB2 and TLR2 mutagenesis primers

646 Supplementary Table S6. Primer list of RT-qPCR

647 Supplementary Table S7. Immunogene panel sequencing result for the index patient

648 Supplementary Table S8. Somatic NFKB2, TLR2 and MTOR mutations in different cellular fractions from the

649 index patient validated by amplicon sequencing

650 Supplementary Table S9. Somatic TLR2 mutation in CD4+ T-cells validated by amplicon sequencing

651

652 Supplementary Table S10. Somatic TLR2 mutation in CD8+ T-cells validated by amplicon sequencing

653

654 Supplementary Table S11. Gene set enrichment analysis (GSEA)

Acknowledgements

Funding: This work was supported by the European Research Council (M-IMM project), Academy of Finland, Finnish special governmental subsidy for health sciences, research and training, Sigrid Juselius Foundation, Instrumentarium Science foundation, Helsinki Institute of Life Sciences Fellow funding, and Finnish Cancer Institute. TL was supported by the Academy of Finland (Decisions 311081 and 314557). This study was supported by Finnish Functional Genomics Centre, University of Turku, Åbo Akademi University and Biocenter Finland.

Author Contributions: G.P., D.K., S.L., R.K., M.K. and S.M. designed the study and experiments. A.M.H., C.M-C., L.C., V.G.G.S., T.H.C-L., A.K., A.J., U.S., and M.I-R. contributed and prepared biological samples and clinical data. G.P., D.K., S.L., R.K., O.B., J.H., and T.L. performed experiments and analyzed the data. P.E. and S.H. designed, supervised and performed sequencing assays. S.E. performed bioinformatic analyses. S.M. conceived and designed the study, directed and supervised research. G.P, M.K., and S.M. wrote the manuscript. All authors read and approved the final manuscript.

Competing Interests statement: S.M. has received honoraria and research funding from Novartis, Pfizer and Bristol-Myers Squibb (not related to this study). The remaining authors declare no competing interests.

Data and materials availability: Patient whole-exome sequencing and RNA-seq data are available from the corresponding author upon suitable request. All other data associated with this study are available in the main text or the supplementary materials.

674 **REFERENCES**

675 1. J. R. Passweg, H. Baldomero, P. Bader, C. Bonini, S. Cesaro, P. Dreger, R. F. Duarte, C. Dufour, J.
676 Kuball, D. Farge-Bancel, A. Gennery, N. Kroger, F. Lanza, A. Nagler, A. Sureda, M. Mohty,
677 Hematopoietic stem cell transplantation in Europe 2014: more than 40 000 transplants annually.
678 *Bone Marrow Transplant* **51**, 786-792 (2016).
679 2. B. R. Blazar, W. J. Murphy, M. Abedi, Advances in graft-versus-host disease biology and therapy.
680 *Nat Rev Immunol* **12**, 443-458 (2012).
681 3. K. R. Cooke, L. Luznik, S. Sarantopoulos, F. T. Hakim, M. Jagasia, D. H. Fowler, M. R. M. van den
682 Brink, J. A. Hansen, R. Parkman, D. B. Miklos, P. J. Martin, S. Paczesny, G. Vogelsang, S. Pavletic,
683 J. Ritz, K. R. Schultz, B. R. Blazar, The Biology of Chronic Graft-versus-Host Disease: A Task
684 Force Report from the National Institutes of Health Consensus Development Project on Criteria for
685 Clinical Trials in Chronic Graft-versus-Host Disease. *Biol Blood Marrow Transplant* **23**, 211-234
686 (2017).
687 4. R. S. Goldszmid, G. Trinchieri, The price of immunity. *Nat Immunol* **13**, 932-938 (2012).
688 5. F. Pandolfi, R. Cianci, F. Casciano, D. Pagliari, T. De Pasquale, R. Landolfi, G. Di Sante, J. T.
689 Kurnick, F. Ria, Skewed T-cell receptor repertoire: more than a marker of malignancy, a tool to
690 dissect the immunopathology of inflammatory diseases. *J Biol Regul Homeost Agents* **25**, 153-161
691 (2011).
692 6. P. Savola, T. Kelkka, H. L. Rajala, A. Kuuliala, K. Kuuliala, S. Eldfors, P. Ellonen, S. Lagstrom, M.
693 Lepisto, T. Hannunen, E. I. Andersson, R. K. Khajuria, T. Jaatinen, R. Koivuniemi, H. Repo, J.
694 Saarela, K. Porkka, M. Leirisalo-Repo, S. Mustjoki, Somatic mutations in clonally expanded
695 cytotoxic T lymphocytes in patients with newly diagnosed rheumatoid arthritis. *Nat Commun* **8**,
696 15869 (2017).
697 7. Y. J. Zhang, Y. Duan, X. F. Zheng, Targeting the mTOR kinase domain: the second generation of
698 mTOR inhibitors. *Drug Discov Today* **16**, 325-331 (2011).
699 8. S. C. Sun, The non-canonical NF-kappaB pathway in immunity and inflammation. *Nat Rev Immunol*
700 **17**, 545-558 (2017).
701 9. U. Platzbecker, J. Stoehlmacher, C. Pabst, E. Goekkurt, U. Oelschlagel, H. Schirutschke, K. Holig,
702 C. Theuser, U. Mogck, G. Ehninger, M. Bornhauser, Induction of Toll-like receptor 2 and 4
703 expression on CD4+ and CD8+ T cells in G-CSF-mobilized unrelated peripheral blood stem cell
704 grafts during leukapheresis: impact on patient outcome. *Leukemia* **22**, 1438-1440 (2008).
705 10. H. L. Rajala, T. Olson, M. J. Clemente, S. Lagstrom, P. Ellonen, T. Lundan, D. E. Hamm, S. A.
706 Zaman, J. M. Lopez Marti, E. I. Andersson, A. Jerez, K. Porkka, J. P. Maciejewski, T. P. Loughran,
707 S. Mustjoki, The analysis of clonal diversity and therapy responses using STAT3 mutations as a
708 molecular marker in large granular lymphocytic leukemia. *Haematologica* **100**, 91-99 (2015).
709 11. H. B. Jefferies, S. Fumagalli, P. B. Dennis, C. Reinhard, R. B. Pearson, G. Thomas, Rapamycin
710 suppresses 5'TOP mRNA translation through inhibition of p70s6k. *EMBO J* **16**, 3693-3704 (1997).
711 12. D. D. Sarbassov, D. A. Guertin, S. M. Ali, D. M. Sabatini, Phosphorylation and regulation of
712 Akt/PKB by the rictor-mTOR complex. *Science* **307**, 1098-1101 (2005).
713 13. B. C. Grabiner, V. Nardi, K. Birsoy, R. Possemato, K. Shen, S. Sinha, A. Jordan, A. H. Beck, D. M.
714 Sabatini, A diverse array of cancer-associated MTOR mutations are hyperactivating and can predict
715 rapamycin sensitivity. *Cancer Discov* **4**, 554-563 (2014).
716 14. S. Gerondakis, T. S. Fulford, N. L. Messina, R. J. Grumont, NF-kappaB control of T cell
717 development. *Nat Immunol* **15**, 15-25 (2014).
718 15. B. Hwang, J. H. Lee, D. Bang, Single-cell RNA sequencing technologies and bioinformatics
719 pipelines. *Exp Mol Med* **50**, 96 (2018).
720 16. J. Glamann, A. J. Hansen, Dynamic detection of natural killer cell-mediated cytotoxicity and cell
721 adhesion by electrical impedance measurements. *Assay Drug Dev Technol* **4**, 555-563 (2006).

722 17. A. Kreutzman, B. Colom-Fernandez, A. M. Jimenez, M. Ilander, C. Cuesta-Mateos, Y. Perez-Garcia,
723 C. D. Arevalo, O. Bruck, H. Hakanen, J. Saarela, A. Ortega-Carrion, A. de Rosendo, A. Juanes-
724 Garcia, J. L. Steegmann, S. Mustjoki, M. Vicente-Manzanares, C. Munoz-Calleja, Dasatinib
725 Reversibly Disrupts Endothelial Vascular Integrity by Increasing Non-Muscle Myosin II
726 Contractility in a ROCK-Dependent Manner. *Clin Cancer Res* **23**, 6697-6707 (2017).
727 18. T. Pemovska, M. Kontro, B. Yadav, H. Edgren, S. Eldfors, A. Szwajda, H. Almusa, M. M. Bespalov,
728 P. Ellonen, E. Elonen, B. T. Gjertsen, R. Karjalainen, E. Kulesskiy, S. Lagstrom, A. Lehto, M.
729 Lepisto, T. Lundan, M. M. Majumder, J. M. Marti, P. Mattila, A. Murumagi, S. Mustjoki, A. Palva,
730 A. Parsons, T. Pirttinen, M. E. Ramet, M. Suvela, L. Turunen, I. Vastrik, M. Wolf, J. Knowles, T.
731 Aittokallio, C. A. Heckman, K. Porkka, O. Kallioniemi, K. Wennerberg, Individualized systems
732 medicine strategy to tailor treatments for patients with chemorefractory acute myeloid leukemia.
733 *Cancer Discov* **3**, 1416-1429 (2013).
734 19. I. Martincorena, P. J. Campbell, Somatic mutation in cancer and normal cells. *Science* **349**, 1483-
735 1489 (2015).
736 20. M. Xie, C. Lu, J. Wang, M. D. McLellan, K. J. Johnson, M. C. Wendl, J. F. McMichael, H. K.
737 Schmidt, V. Yellapantula, C. A. Miller, B. A. Ozenberger, J. S. Welch, D. C. Link, M. J. Walter, E.
738 R. Mardis, J. F. Dipersio, F. Chen, R. K. Wilson, T. J. Ley, L. Ding, Age-related mutations
739 associated with clonal hematopoietic expansion and malignancies. *Nat Med* **20**, 1472-1478 (2014).
740 21. E. Holzelova, C. Vonarbourg, M. C. Stolzenberg, P. D. Arkwright, F. Selz, A. M. Prieur, S. Blanche,
741 J. Bartunkova, E. Vilmer, A. Fischer, F. Le Deist, F. Rieux-Laucat, Autoimmune lymphoproliferative
742 syndrome with somatic Fas mutations. *N Engl J Med* **351**, 1409-1418 (2004).
743 22. K. A. Ross, Coherent somatic mutation in autoimmune disease. *PLoS One* **9**, e101093 (2014).
744 23. S. I. Nikolaev, S. Vetiska, X. Bonilla, E. Boudreau, S. Jauhiainen, B. Rezai Jahromi, N. Khyzha, P.
745 V. DiStefano, S. Suutarinen, T. R. Kiehl, V. Mendes Pereira, A. M. Herman, T. Krings, H. Andrade-
746 Barazarte, T. Tung, T. Valiante, G. Zadeh, M. Tymianski, T. Rauramaa, S. Yla-Herttuala, J. D.
747 Wythe, S. E. Antonarakis, J. Frosen, J. E. Fish, I. Radovanovic, Somatic Activating KRAS Mutations
748 in Arteriovenous Malformations of the Brain. *N Engl J Med* **378**, 250-261 (2018).
749 24. H. L. Koskela, S. Eldfors, P. Ellonen, A. J. van Adrichem, H. Kuusanmaki, E. I. Andersson, S.
750 Lagstrom, M. J. Clemente, T. Olson, S. E. Jalkanen, M. M. Majumder, H. Almusa, H. Edgren, M.
751 Lepisto, P. Mattila, K. Guinta, P. Koistinen, T. Kuittinen, K. Penttinen, A. Parsons, J. Knowles, J.
752 Saarela, K. Wennerberg, O. Kallioniemi, K. Porkka, T. P. Loughran, Jr., C. A. Heckman, J. P.
753 Maciejewski, S. Mustjoki, Somatic STAT3 mutations in large granular lymphocytic leukemia. *N*
754 *Engl J Med* **366**, 1905-1913 (2012).
755 25. J. A. Fraietta, C. L. Nobles, M. A. Sammons, S. Lundh, S. A. Carty, T. J. Reich, A. P. Cogdill, J. J.
756 D. Morrissette, J. E. DeNizio, S. Reddy, Y. Hwang, M. Gohil, I. Kulikovskaya, F. Nazimuddin, M.
757 Gupta, F. Chen, J. K. Everett, K. A. Alexander, E. Lin-Shiao, M. H. Gee, X. Liu, R. M. Young, D.
758 Ambrose, Y. Wang, J. Xu, M. S. Jordan, K. T. Marcucci, B. L. Levine, K. C. Garcia, Y. Zhao, M.
759 Kalos, D. L. Porter, R. M. Kohli, S. F. Lacey, S. L. Berger, F. D. Bushman, C. H. June, J. J.
760 Melenhorst, Disruption of TET2 promotes the therapeutic efficacy of CD19-targeted T cells. *Nature*
761 **558**, 307-312 (2018).
762 26. F. Janku, T. A. Yap, F. Meric-Bernstam, Targeting the PI3K pathway in cancer: are we making
763 headway? *Nat Rev Clin Oncol* **15**, 273-291 (2018).
764 27. B. Blanco, M. C. Herrero-Sanchez, C. Rodriguez-Serrano, M. Sanchez-Barba, M. C. Del Canizo,
765 Profound blockade of T cell activation requires concomitant inhibition of different class I PI3K
766 isoforms. *Immunol Res* **62**, 175-188 (2015).
767 28. A. Abouelnasr, J. Roy, S. Cohen, T. Kiss, S. Lachance, Defining the role of sirolimus in the
768 management of graft-versus-host disease: from prophylaxis to treatment. *Biol Blood Marrow*
769 *Transplant* **19**, 12-21 (2013).
770 29. J. A. DiDonato, F. Mercurio, M. Karin, NF-kappaB and the link between inflammation and cancer.
771 *Immunol Rev* **246**, 379-400 (2012).

30. Q. Zhang, M. J. Lenardo, D. Baltimore, 30 Years of NF-kappaB: A Blossoming of Relevance to Human Pathobiology. *Cell* **168**, 37-57 (2017).
31. F. Christian, E. L. Smith, R. J. Carmody, The Regulation of NF-kappaB Subunits by Phosphorylation. *Cells* **5**, (2016).
32. T. H. Flo, O. Halaas, S. Torp, L. Ryan, E. Lien, B. Dybdahl, A. Sundan, T. Espevik, Differential expression of Toll-like receptor 2 in human cells. *J Leukoc Biol* **69**, 474-481 (2001).
33. M. Komai-Koma, L. Jones, G. S. Ogg, D. Xu, F. Y. Liew, TLR2 is expressed on activated T cells as a costimulatory receptor. *Proc Natl Acad Sci U S A* **101**, 3029-3034 (2004).
34. S. P. Cullen, M. Brunet, S. J. Martin, Granzymes in cancer and immunity. *Cell Death Differ* **17**, 616-623 (2010).
35. D. M. Brown, A. T. Lampe, A. M. Workman, The Differentiation and Protective Function of Cytolytic CD4 T Cells in Influenza Infection. *Front Immunol* **7**, 93 (2016).
36. H. Cheroutre, M. M. Husain, CD4 CTL: living up to the challenge. *Semin Immunol* **25**, 273-281 (2013).
37. V. S. Patil, A. Madrigal, B. J. Schmiedel, J. Clarke, P. O'Rourke, A. D. de Silva, E. Harris, B. Peters, G. Seumois, D. Weiskopf, A. Sette, P. Vijayanand, Precursors of human CD4(+) cytotoxic T lymphocytes identified by single-cell transcriptome analysis. *Sci Immunol* **3**, (2018).
38. W. Wei, Y. Jiao, A. Postlethwaite, J. M. Stuart, Y. Wang, D. Sun, W. Gu, Dual-specificity phosphatases 2: surprising positive effect at the molecular level and a potential biomarker of diseases. *Genes Immun* **14**, 1-6 (2013).
39. D. Lu, L. Liu, X. Ji, Y. Gao, X. Chen, Y. Liu, Y. Liu, X. Zhao, Y. Li, Y. Li, Y. Jin, Y. Zhang, M. A. McNutt, Y. Yin, The phosphatase DUSP2 controls the activity of the transcription activator STAT3 and regulates TH17 differentiation. *Nat Immunol* **16**, 1263-1273 (2015).
40. R. Lang, M. Hammer, J. Mages, DUSP meet immunology: dual specificity MAPK phosphatases in control of the inflammatory response. *J Immunol* **177**, 7497-7504 (2006).
41. A. M. Fischer, C. D. Katayama, G. Pages, J. Pouyssegur, S. M. Hedrick, The role of erk1 and erk2 in multiple stages of T cell development. *Immunity* **23**, 431-443 (2005).
42. X. He, R. L. Smeets, H. J. Koenen, P. M. Vink, J. Wagenaars, A. M. Boots, I. Joosten, Mycophenolic acid-mediated suppression of human CD4+ T cells: more than mere guanine nucleotide deprivation. *Am J Transplant* **11**, 439-449 (2011).
43. D. A. Guertin, D. M. Sabatini, Defining the role of mTOR in cancer. *Cancer Cell* **12**, 9-22 (2007).
44. C. K. Tsang, H. Qi, L. F. Liu, X. F. Zheng, Targeting mammalian target of rapamycin (mTOR) for health and diseases. *Drug Discov Today* **12**, 112-124 (2007).
45. M. A. Bjornsti, P. J. Houghton, The TOR pathway: a target for cancer therapy. *Nat Rev Cancer* **4**, 335-348 (2004).
46. A. Perl, mTOR activation is a biomarker and a central pathway to autoimmune disorders, cancer, obesity, and aging. *Ann N Y Acad Sci* **1346**, 33-44 (2015).
47. X. F. Zheng, D. Florentino, J. Chen, G. R. Crabtree, S. L. Schreiber, TOR kinase domains are required for two distinct functions, only one of which is inhibited by rapamycin. *Cell* **82**, 121-130 (1995).
48. M. E. Feldman, B. Apsel, A. Uotila, R. Loewith, Z. A. Knight, D. Ruggero, K. M. Shokat, Active-site inhibitors of mTOR target rapamycin-resistant outputs of mTORC1 and mTORC2. *PLoS Biol* **7**, e38 (2009).
49. C. C. Thoreen, S. A. Kang, J. W. Chang, Q. Liu, J. Zhang, Y. Gao, L. J. Reichling, T. Sim, D. M. Sabatini, N. S. Gray, An ATP-competitive mammalian target of rapamycin inhibitor reveals rapamycin-resistant functions of mTORC1. *J Biol Chem* **284**, 8023-8032 (2009).
50. M. Taipale, D. F. Jarosz, S. Lindquist, HSP90 at the hub of protein homeostasis: emerging mechanistic insights. *Nat Rev Mol Cell Biol* **11**, 515-528 (2010).
51. Y. Fukuyo, C. R. Hunt, N. Horikoshi, Geldanamycin and its anti-cancer activities. *Cancer Lett* **290**, 24-35 (2010).

822 52. P. C. Echeverria, A. Bernthaler, P. Dupuis, B. Mayer, D. Picard, An interaction network predicted
823 from public data as a discovery tool: application to the Hsp90 molecular chaperone machine. *PLoS*
824 *One* **6**, e26044 (2011).
825 53. G. M. Delgoffe, T. P. Kole, R. J. Cotter, J. D. Powell, Enhanced interaction between Hsp90 and
826 raptor regulates mTOR signaling upon T cell activation. *Mol Immunol* **46**, 2694-2698 (2009).
827 54. S. Sato, N. Fujita, T. Tsuruo, Modulation of Akt kinase activity by binding to Hsp90. *Proc Natl Acad*
828 *Sci U S A* **97**, 10832-10837 (2000).
829 55. H. Bekki, K. Kohashi, A. Maekawa, Y. Yamada, H. Yamamoto, K. Harimaya, M. Hakozaki, K.
830 Nabeshima, Y. Iwamoto, Y. Oda, Elevated expression of HSP90 and the antitumor effect of an
831 HSP90 inhibitor via inactivation of the Akt/mTOR pathway in undifferentiated pleomorphic
832 sarcoma. *BMC Cancer* **15**, 804 (2015).
833 56. L. Giulino-Roth, H. J. van Besien, T. Dalton, J. E. Totonchy, A. Rodina, T. Taldone, A. Bolaender,
834 H. Erdjument-Bromage, J. Sadek, A. Chadburn, M. J. Barth, F. S. Dela Cruz, A. Rainey, A. L. Kung,
835 G. Chiosis, E. Cesarman, Inhibition of Hsp90 Suppresses PI3K/AKT/mTOR Signaling and Has
836 Antitumor Activity in Burkitt Lymphoma. *Mol Cancer Ther* **16**, 1779-1790 (2017).
837 57. Q. Huang, S. He, Y. Tian, Y. Gu, P. Chen, C. Li, J. Huang, Y. Liu, H. Yu, M. Jin, S. Hu, Q. Tong, A.
838 Ma, J. Jin, E. Hexner, H. Fung, R. Reshef, Y. Zhang, Y. Zhang, Hsp90 inhibition destabilizes Ezh2
839 protein in alloreactive T cells and reduces graft-versus-host disease in mice. *Blood* **129**, 2737-2748
840 (2017).
841 58. C. S. Carlson, R. O. Emerson, A. M. Sherwood, C. Desmarais, M. W. Chung, J. M. Parsons, M. S.
842 Steen, M. A. LaMadrid-Herrmannsfeldt, D. W. Williamson, R. J. Livingston, D. Wu, B. L. Wood,
843 M. J. Rieder, H. Robins, Using synthetic templates to design an unbiased multiplex PCR assay. *Nat*
844 *Commun* **4**, 2680 (2013).
845 59. C. Soneson, M. D. Robinson, Bias, robustness and scalability in single-cell differential expression
846 analysis. *Nat Methods* **15**, 255-261 (2018).
847 60. M. Vangipuram, D. Ting, S. Kim, R. Diaz, B. Schule, Skin punch biopsy explant culture for
848 derivation of primary human fibroblasts. *J Vis Exp*, e3779 (2013).
849 61. B. Yadav, T. Pemovska, A. Szwajda, E. Kulesskiy, M. Kontro, R. Karjalainen, M. M. Majumder, D.
850 Malani, A. Murumagi, J. Knowles, K. Porkka, C. Heckman, O. Kallioniemi, K. Wennerberg, T.
851 Aittokallio, Quantitative scoring of differential drug sensitivity for individually optimized anticancer
852 therapies. *Sci Rep* **4**, 5193 (2014).
853
854
855

856 **Table 1. Somatic mutations discovered in CD4+ T cells in the index patient, detected from 2013 sample**

Chr	position	ref	var	Gene	Mutation type	Codon change	Exon	Amino acid change	Normal_ Ref reads [1]	Normal_ Alt reads [2]	Normal_var_ Freq (%)	Tumor_ Ref reads [3]	Tumor_ Alt reads [4]	Tumor_var_ Freq (%)	Somatic p-value [*]
1	11182160	G	C	*MTOR*	MISSENSE	cCt/cGt	48	P2229R	179	8	4.28	157	24	13.26	0.0017815
4	154625732	G	T	*TLR2*	MISSENSE	tGg/tTg	1	W558L	116	2	1.69	104	10	8.77	0.014504
4	144801662	C	G	*GYPE*	MISSENSE	gGa/gCa	2	G13A	150	68	31.19	147	99	40.24	0.026604
19	50017643	G	T	*FCGRT*	MISSENSE	caG/caT	3	Q167H	28	0	0	14	2	12.5	0.12685
16	31388150	A	G	*ITGAX*	MISSENSE	Aca/Gca	21	T847A	57	0	0	35	2	5.41	0.15237
11	2415324	G	T	*CD81*	SPLICING		4		58	0	0	36	2	5.26	0.15417
22	37326772	C	A	*CSF2RB*	MISSENSE	caC/caA	8	H310Q	54	0	0	35	2	5.41	0.16264
3	49936028	A	C	*MST1R*	MISSENSE	Tgt/Ggt	4	C548G	45	0	0	38	2	5	0.21849
10	104162075	C	A	*NFKB2*	MISSENSE	cCa/cAa	23	P882Q	14	0	0	26	3	10.34	0.29609
10	18112382	G	T	*MRC1*	MISSENSE	Ggt/Tgt	2	G134C	29	0	0	35	2	5.41	0.31049
17	80274159	G	GT	*CD7*	FRAME SHIFT	gca/gAca	3	A175D?	8	0	0	16	3	15.79	0.33128
17	80274183	G	C	*CD7*	MISSENSE	gCc/gGc	3	A167G	13	0	0	19	2	9.52	0.37433
12	109017698	G	A	*SELPLG*	MISSENSE	aCg/aTg	2	T145M	46	2	4.17	35	3	7.89	0.38939
17	80274161	TG	T	*CD7*	FRAME SHIFT	-/-	3		7	0	0	11	2	15.38	0.41053

857

858 Immunogene panel sequencing was performed on both CD4+ and CD8+ T cells from the index cGvHD

859 patient. The table shows discovered somatic mutations in the expanded CD4+ T cells.

860

861 Abbreviations: Chr, chromosome; ref, reference base; var, variant base; freq, frequency

862 [1] Sequencing reads supporting reference allele in normal sample, [2] Sequencing reads supporting variant

863 allele in normal sample, [3] Sequencing reads supporting reference allele in tumor sample, [4] Sequencing

864 reads supporting variant allele in tumor sample, [*] Somatic p-value for somatic/loss of heterozygosity

865 events

866 **Table 2. Somatic *MTOR* and *NFkB2* mutations validated by amplicon sequencing**

Sample year	Patient	DNAs	Gene	Chr	position	ref	var	Amino acid change	Call_Depth	Ref_Calls	Var_Calls	VAF (%)	Freq_Ratio
2015	1-1	CD4+ T	*MTOR*	1	112182160	G	C	P2229R	1000004	808220	191784	**19.2**	1.00047
2015	1-2	CD8+T	*MTOR*	1	112182160	G	C	P2229R	1000003	942683	57320	**5.7**	0.9993
2017	1-3	CD4+ Vb.20+	*MTOR*	1	112182160	G	C	P2229R	168592	93183	75409	**44.7**	0.99928
2017	1-4	CD4+CD8+ Vb.20+	*MTOR*	1	112182160	G	C	P2229R	171728	110670	61058	**35.5**	0.99910
2015	1-5	Skin-biopsy	*MTOR*	1	112182160	G	C	P2229R	8085	7986	99	**0.8**	0.96305
2016	2	Whole blood	*MTOR*	1	112182160	G	C	P2229R	2743	2715	28	**1.0**	1.01793
2015	3	Whole blood	*MTOR*	1	112182160	G	C	P2229R	719	703	16	**2.0**	1.02671
2015	1-1	CD4+T	*NFkB2*	10	104162075	C	A	P882Q	471375	414821	56554	**12.0**	1.0061
2015	1-2	CD8+T	*NFkB2*	10	104162075	C	A	P882Q	586903	577283	9620	**1.6**	1.00124
2017	1-3	CD4+ Vb.20+	*NFkB2*	10	104162075	C	A	P882Q	26262	20668	5594	**21.3**	1.00395
2017	1-4	CD4+CD8+ Vb.20+	*NFkB2*	10	104162075	C	A	P882Q	48654	43822	4832	**9.9**	1.00282

867

868 CD4+ and CD8+ T cells were sorted either with the magnetic beads (2015 sample) or flow based sorting
869 (2017 sample). In addition, CD4+Vb20+ and CD4+CD8+Vb20+ fractions were sorted with flow cytometry
870 (2017 sample). *MTOR* and *NFkB2* mutations were analysed from sorted fractions with deep amplicon
871 sequencing. Mutations were confined to CD4+ fractions. The low mutation VAFs in CD8+ fraction are due
872 to small CD4+ T cell contamination (CD4+CD8+ double positive cells) in the bead sorted fraction.

873

874 Abbreviations: Chr, chromosome; ref, reference base; var, variant base; Call_depth, total number of called
875 reads; Ref_calls, sequencing reads supporting reference allele; Var_calls, sequencing reads supporting
876 variant allele; VAF, variant allele frequency; Freq, frequency; Freq_Ratio, base quality frequency ratio.

877

878

879 **Figure 1.**

880

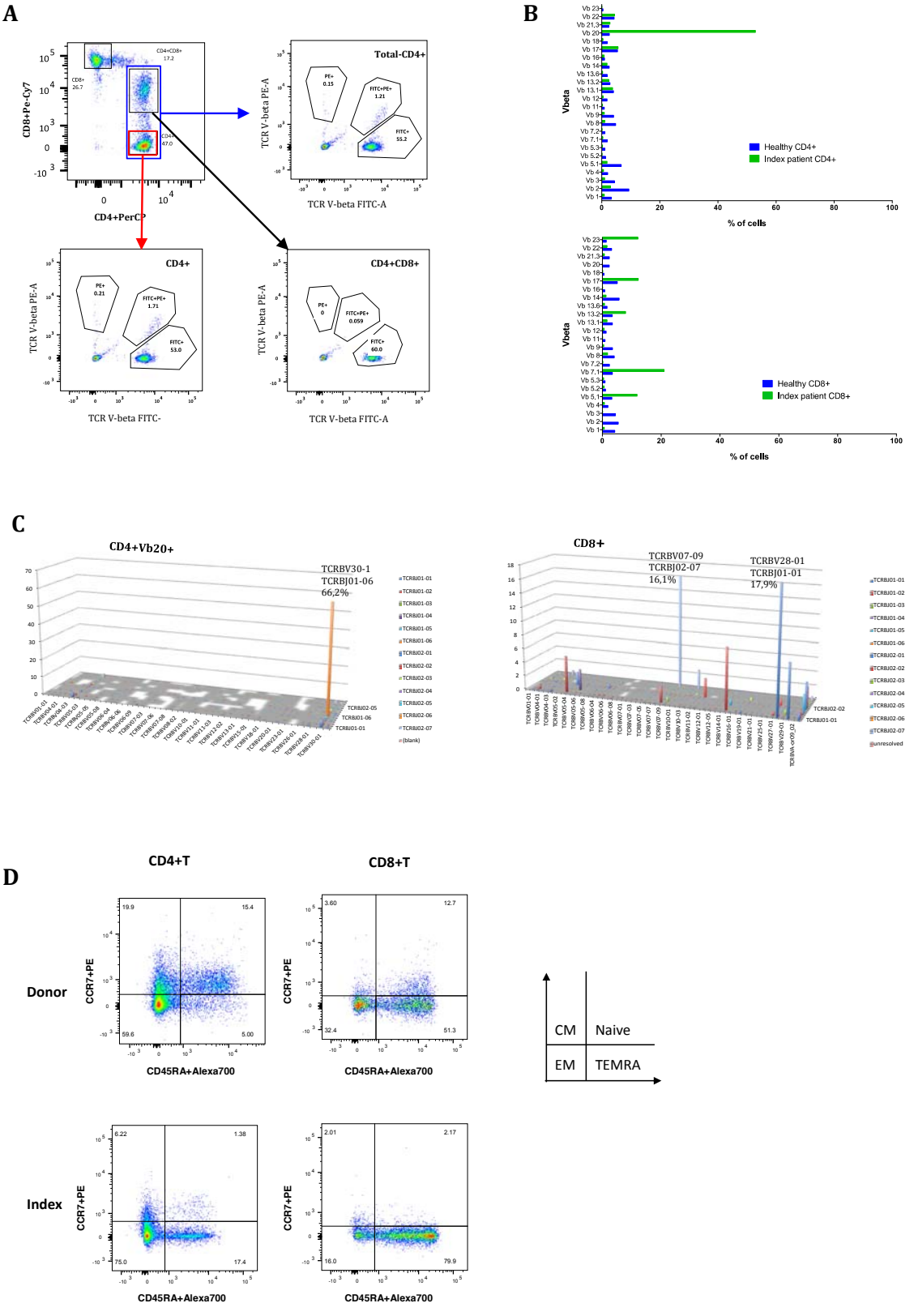

881 **Figure 1**. **Flow cytometry and TCRB deep sequencing results from the index patient**.

882 (A) and (B). TCR Vβ repertoire of CD4+ and CD8+ T cells was analyzed in peripheral
883 blood from the Index patient with the IO Test Beta Mark TCR beta Repertoire Kit
884 (Beckman-Coulter Immunotech, USA). 53% of CD4+T cells and 60% of CD4+CD8+T
885 cells consisted of a single Vβ20 clone.
886 (C) T cell repertoire of FACS-sorted CD4+Vβ20+ and CD8+ T cells analysed with TCRβ
887 deep sequencing (Adaptive Biotech., USA). The TCRBV30-01 clone was detected in
888 the CD4+Vβ20+ fraction, but not in the CD8+ fraction.
889 (D) Multicolor flow cytometry was applied to identify the immune phenotype of
890 donor and index patient's memory T cell subtypes. Central memory (CM), naïve,
891 effector memory (EM) and terminal effector memory (TEMRA) cells.
892
893

894 **Figure 2.**

895 **A**

896 **mTOR**

897

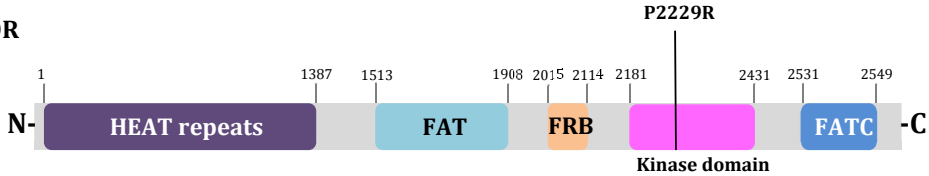

NFkB2

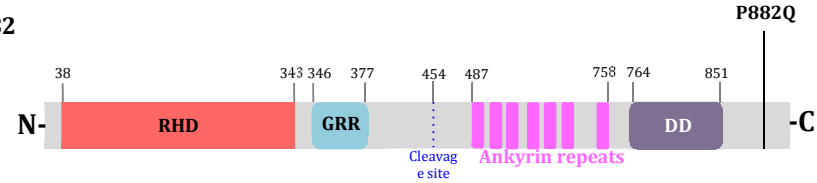

TLR2

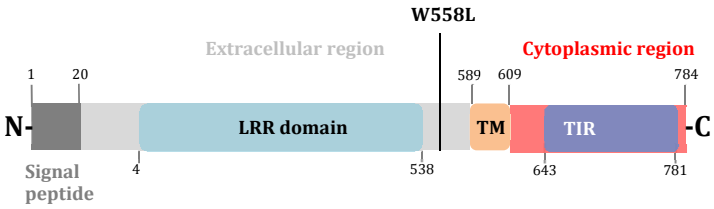

B

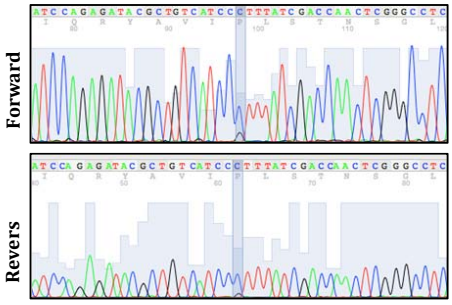

C

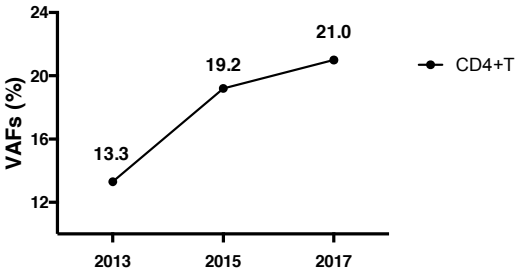

D

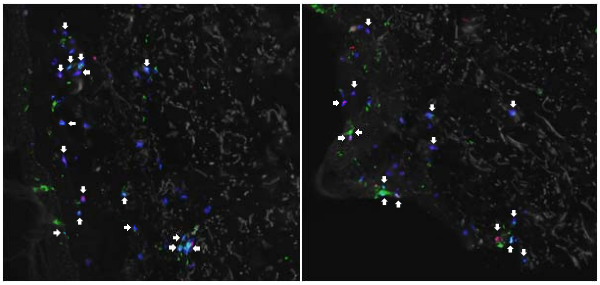

898 **Figure 2. *MTOR, NFkB2*, and *TLR2* mutations in index patient**

899 (A) Locations of *MTOR, TLR2,* and *NFkB2* somatic mutations. Linearized structure of
900 MTOR, NFkB2, and TLR2 presenting the location of somatic mutations. *MTOR*
901 *P2229R* mutation is located in the kinase domain, *NFkB2 P882Q* in the C-terminus,
902 and *TLR2 W558L* between LRR (Leucine-rich repeats) domain and transmembrane
903 (TM) domain.

904 (B) A heterozygous *MTOR* mutation (G to C, P2229R) was detected in CD4+ T cells by
905 Sanger sequencing.

906 (C) Variant allele frequencies (VAFs) of *MTOR* mutation in the index patient's CD4+ T
907 cells over time as measured with amplicon sequencing.

908 (D) Immunofluorescence staining indicated CD3+CD4+ and CD3+CD8+T cell
909 infiltration in the skin. Paraffin embedded skin biopsy from index patient was
910 sectioned and stained with antibody specific human CD3 (cyan), CD4 (green), and
911 CD8 (red). White arrows indicate infiltrated CD3+CD4+ or CD3+CD8+T cells.

912

913 **Figure 3.**

914 **A**

915

916

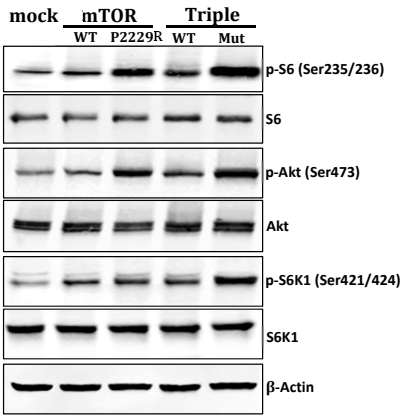

B

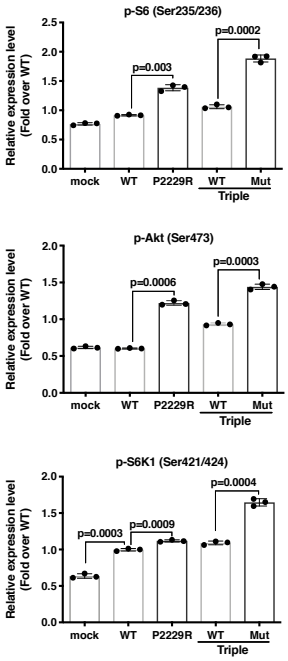

C

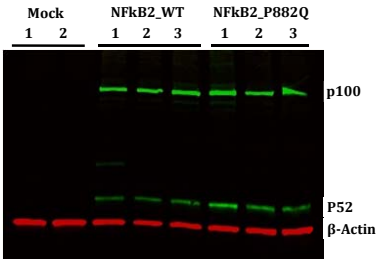

D

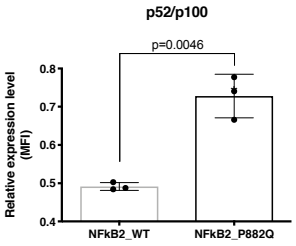

917 **Figure 3. Functional analysis for wild type, *MTOR,* and *NFkB2* mutants in HEK293**
918 **cells**
919 (A) Stably expressed *MTOR* wildtype (WT), mutant (P2229R), Triple (*MTOR, TLR2,*
920 and *NFKB2*) wildtype (WT) and Triple mutant (*MTOR P2229R*, *TLR2 W559L*, and
921 *NFKB2 P882Q*) (Mut) in HEK293 cells were serum starved for 12 hours. Western blot
922 analysis was performed with the use of anti-pS6, anti-S6, anti-pAkt, anti-Akt, anti-
923 pS6K1, anti-S6K1, and anti-β-actin. Data is representative of three independent
924 experiments.
925 (B) Relative expression level was estimated by measuring each band intensity of
926 three independent experiments using ImageJ software (Rasband, W.S., ImageJ, U. S.
927 National Institutes of Health, Bethesda, Maryland, USA, https://imagej.nih.gov/ij/,
928 1997-2016). Error bar present Mean ± SEM (n=3 per group). P values are derived
929 from unpaired t-test with Welch's correction (WT vs P2229R, WT vs Triple Mut, and
930 mock vs WT in p-S6K1).
931 (C) Immonoblot assay was performed to verify an alteration of P52 and P100
932 expression with *NFkB2* WT and *P882Q* mutant. Data is representative of three
933 independent experiments.
934 (D) Stably expressing *NFkB2 P882Q* increased expression of P52. Mean fluorescence
935 intensity was measured by ImageJ software (NFkB2_WT: n =3, NFkB2_P882Q: n=3).
936 Error bar present Mean ± SEM. P values are derived from unpaired t-test with
937 Welch's correction (NFkB2_WT vs NFkB2_P882Q).
938

Figure 4.

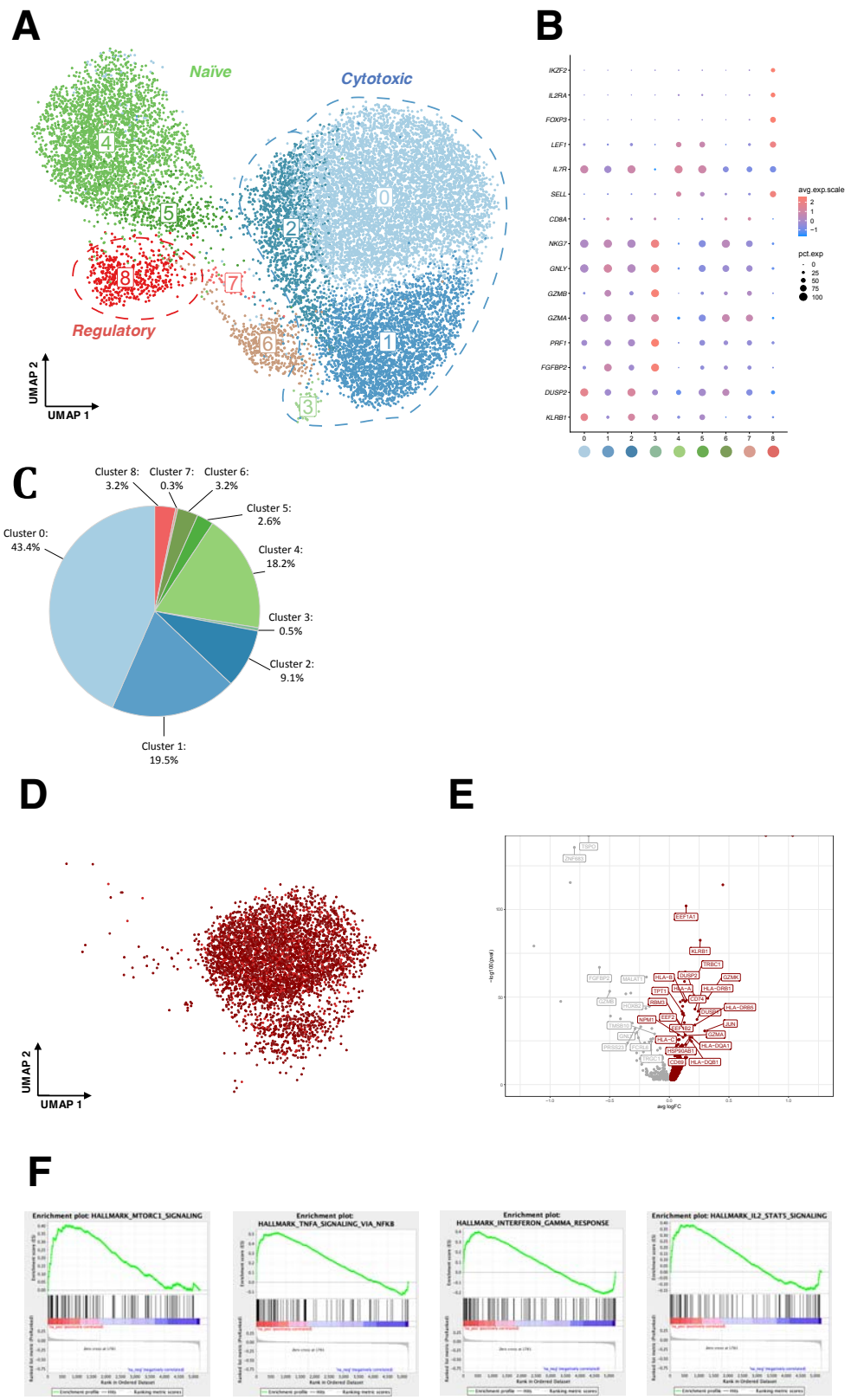
A
Naïve
Cytotoxic
Regulatory
UMAP 2
UMAP 1
B
IKZF2
IL2RA
FOXP3
LEF1
IL7R
SELL
CD8A
NKG7
GNLY
GZMB
GZMA
PRF1
FGFBP2
DUSP2
KLRB1
avg.exp.scale
pct.exp
C
Cluster 8: 3.2%
Cluster 7: 0.3%
Cluster 6: 3.2%
Cluster 5: 2.6%
Cluster 4: 18.2%
Cluster 3: 0.5%
Cluster 2: 9.1%
Cluster 1: 19.5%
Cluster 0: 43.4%
D
UMAP 2
UMAP 1
E
avg logFC
F
Enrichment plot: HALLMARK_MTORC1_SIGNALING
Enrichment plot: HALLMARK_TNFA_SIGNALING_VIA_NFKB
Enrichment plot: HALLMARK_INTERFERON_GAMMA_RESPONSE
Enrichment plot: HALLMARK_IL2_STAT5_SIGNALING

963 **Figure 4. Single-cell RNAseq analysis from the index patient.**

964 (A) Two-dimension UMAP-projection of clustered CD4+ cells pooled from two time
965 points from peripheral blood. A total of 15,874 cells are annotated in 9 distinct
966 clusters.

967 B) Gene expression heatmap for the 9 distinct CD4+ clusters, where rows represent
968 canonical marker genes and columns represent different clusters

969 C) Pie chart showing the fractions of cells belonging to different clusters. The
970 fractions are pooled from two time points.

971 D) Graphical visualisation showing the cells taken into differential expression
972 analysis. Red shows the clonally expanded and mutated clonotype, and grey cells
973 represent the cells from other clonotypes with similar phenotype

974 E) Volcano plot showing differentially expressed genes between clonotype of
975 interest and cells from other clonotypes with similar phenotype

976 F) Gene Set Enrichment Analysis results from the differential expression analysis.
977 Shown here are four of eleven HALLMARK-categories enriched (FDR qval < 0.05) to
978 clonotype of interest.

979

980

981 **Figure 5.**

982 **A**

983

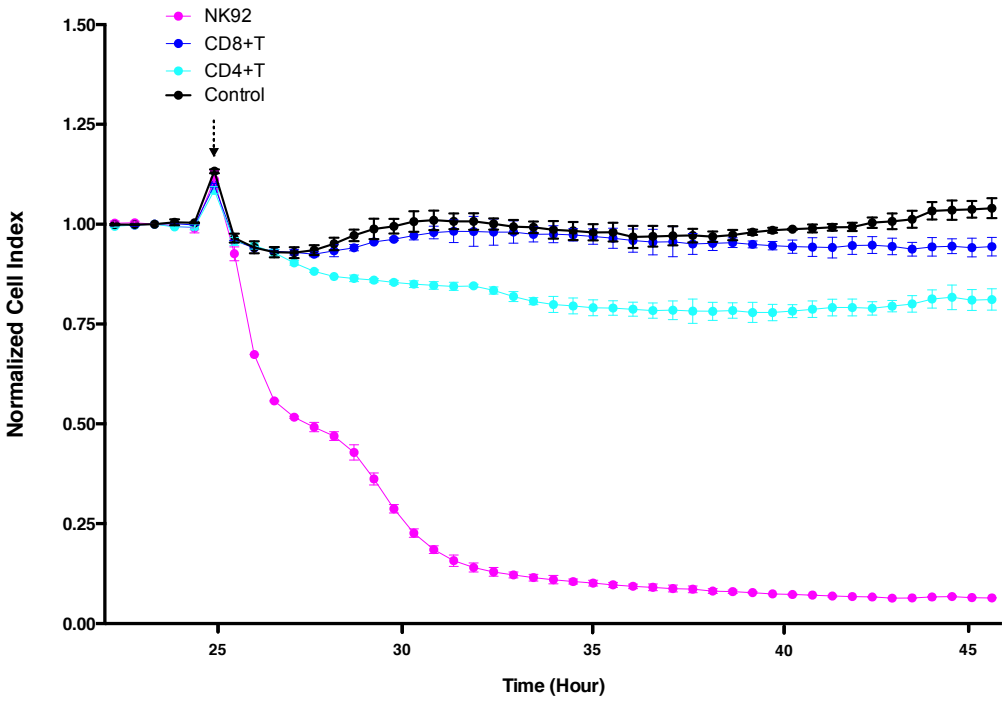

B

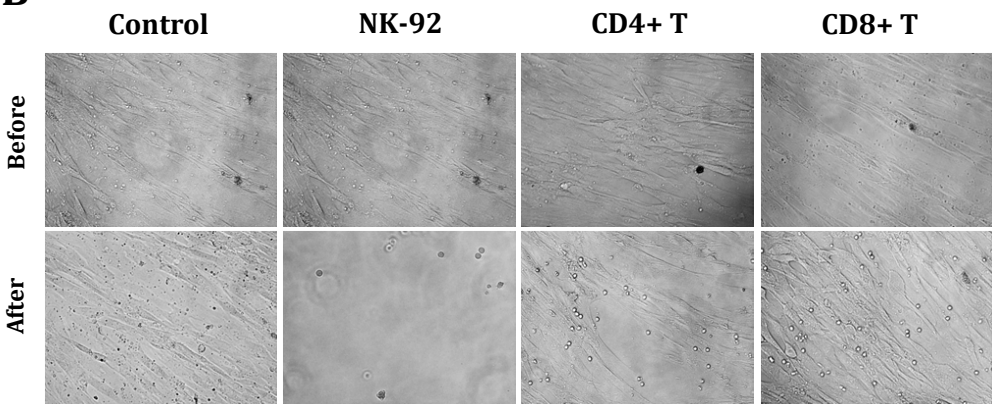

984 **Figure 5. Real-time monitoring of cellular cytotoxicity by electrical impedance**
985 **measurement.** Real-time cell analysing (RTCA) systems, xCELLigence^{TM}, was applied
986 to monitor real-time killing effect of primary fibroblasts obtained from the index
987 patient.
988 A) The primary fibroblasts were cultured as monolayers for 24 hours to reach full
989 confluence. Once confluent, the effector cells; NK-92 cell line (positive control; pink
990 line), primary CD4+ T cells (light blue) and primary CD8+ T cells (dark blue) were
991 added to each well and co-cultured (Arrow). The control (black line) shows the
992 impedance of the fibroblasts without any added effectors. The cell impedance was
993 measured every 30 minutes for 48 hours. The measured impedance was expressed
994 as Cell Index with the normalization (n=2). Data is representative of two
995 independent experiments showing similar results. The curve represents the mean
996 Cell Index value from 2 separate wells ± SD.
997 B) Monolayers of the primary fibroblast were visualized before the addition of the
998 effector cells by inverted microscope (Nikon Eclipse TS100)(upper panels). In the end
999 of the experiment, each well was washed with PBS to photograph the live and still
1000 attached fibroblast.

1001 **Figure 6.**

1002

1003

1004

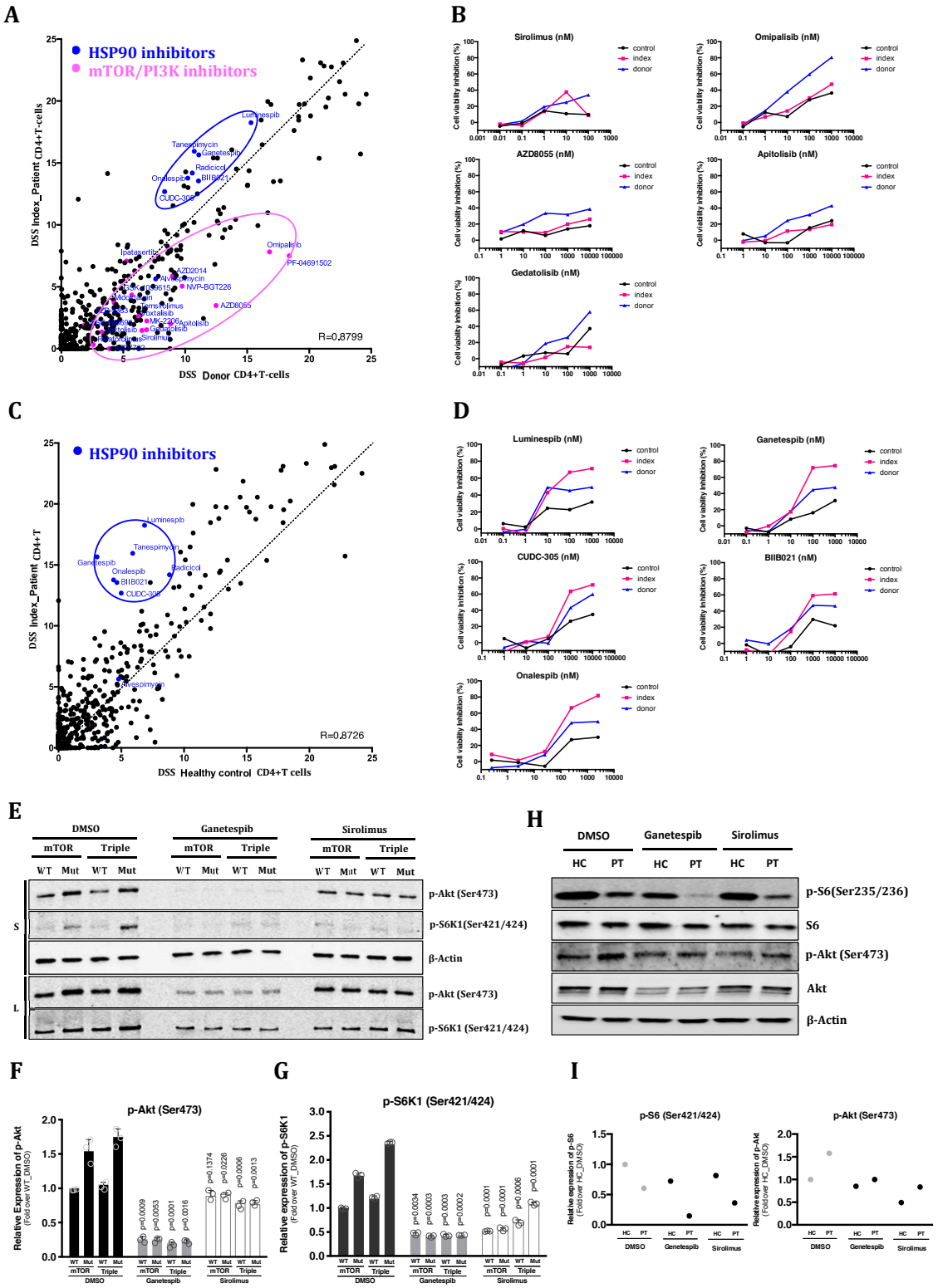

1005 **Figure 6. Drug Sensitivity and Resistance testing (DSRT) of CD4+T cells from index**
1006 **patient compared with CD4+T cells from both healthy control and sibling donor.**
1007 *Ex vivo* DSRT was performed on fresh CD4+T cells from index patient, donor, and
1008 healthy control. Correlation of drug sensitivity scores (DSS) indicating cell viability
1009 inhibition measured by CellTiter-Glo 2.0 (Promega, USA). DSS is a quantitative
1010 measurement of a drug response based on the area under the curve (AUC) with
1011 further normalization. Higher DSS denote better killing activity.
1012 A) Correlation of DSS scores between index patient and donor CD4+ T cells.
1013 B) Individual dose response curves of index patient, donor, and healthy control CD4+
1014 T cells for MTOR inhibitors
1015 C) Correlation of DSS scores between index patient and healthy control CD4+ T cells.
1016 D) Individual dose response curves of index patient, donor, and healthy control CD4+
1017 T cells for HSP90 inhibitors
1018 (E) Stably expressed *MTOR* wildtype (WT), mutant (*P2229R*), Triple (*MTOR, TLR2* and
1019 *NFKB2*) wildtype (*WT*) and Triple mutant (*MTOR P2229R*, *TLR2 W559L*, and *NFKB2*
1020 *P882Q*) (Mut) in HEK293 cells were treated with HSP90 inhibitor (Ganetespib,
1021 100nM) or mTOR inhibitor (Sirolimus, 100nM) for 12 hours. Western blot analysis
1022 was performed with the use of anti-pAkt, anti-pS6K1, and anti-β-actin antibodies.
1023 Different amount of total protein was loaded in the upper panel (S, 30 ug) and the
1024 lower panel (L, 50 ug). Data is representative of three independent experiments.
1025 (F and G) Relative expression levels of phospho-Akt (F) and phospho-S6K1 (G) were
1026 estimated by measuring each band intensity using ImageJ software (Rasband, W.S.,
1027 ImageJ, U. S. National Institutes of Health, Bethesda, Maryland, USA,
1028 https://imagej.nih.gov/ij/, 1997-2016). Mean ± SEM are shown (n=3 for group). P

1029 values are derived from unpaired t-test with Welch's correction (p value on each bar
1030 indicates statistical significance between DMSO and Ganetespib/Sirolimus).
1031 (H) Isolated CD4+T cells from healthy control (HC) and index patient (PT) were
1032 treated with HSP90 inhibitor (Ganetespib, 100nM) or mTOR inhibitor (Sirolimus,
1033 100nM) for 12 hours. Cells were lysed and proteins (25ug of total protein) were run
1034 on the SDS-PAGE gel. Western blot analysis was performed with the use of anti-S6,
1035 anti-pS6, anti-Akt, anti-pAkt and anti-β-actin antibodies.
1036 I) Relative expression levels of phospho-Akt and phospho-S6 were estimated by
1037 measuring band intensity with ImageJ software.
1038
1039